THESIS

SHEAR STRENGTH OF COAL COMBUSTION PRODUCT BY VANE SHEAR

Submitted by

Wesley J. Herweynen

Department of Civil & Environmental Engineering

In partial fulfillment of the requirements

For the Degree of Master of Science

Colorado State University

Fort Collins, Colorado

Summer 2018

Masters Committee:

      Advisor: Christopher A. Bareither
      Co-Advisor: Joseph Scalia

      John Ridley

ABSTRACT

SHEAR STRENGTH OF COAL COMBUSTION PRODUCT BY VANE SHEAR

The objective of this study was to evaluate the shear strength of a coal combustion product (CCP) using the vane shear test. The CCP was obtained from a CCP evaporation pond in the Eastern United States, and consisted primarily of silt-sized particles. A series of small-scale vane shear (diameter = 12.5 mm and height = 25 mm) and large-scale vane shear (diameter = 25 mm and height = 50 mm) tests were conducted on CCP. Undrained and drained strength envelopes were determined for CCP using consolidated undrained (CU) triaxial compression tests. Triaxial results were verified via consolidated drained (CD) direct shear tests on similarly prepared CCP specimens and comparing the results with the drained strength envelope. In addition, effects of the following variables on the vane shear strength of CCP were evaluated using the small-scale vane: (i) rate of vane rotation, (ii) time delay between vane insertion and beginning rotation (t_d), and (iii) elapsed time under the final vertical effective stress prior to shearing (t_c). A fine synthetic tailing (FST), which was 100% fine grained with approximately 40% clay-sized particles, was evaluated for comparison via small-scale vane shear. FST was selected as the higher clay content and lower permeability, relative to CCP, made the material more suited for evaluating vane shear with undrained conditions. All test specimens were prepared in the laboratory via the slurry deposition method and consolidated to the target vertical effective stress.

Vane shear strength results were compared to drained and undrained strength envelopes for CCP and FST. Vane shear strength results were represented in terms of peak shear strength and the initial horizontal effective stress acting on the vertical-oriented failure surface during vane shear. Vane shear tests on CCP in small-scale vane shear and large-scale vane shear yielded shear strengths that plotted between the drained and undrained strength envelopes. This was explained by the small diameter of the vane and/or high permeability of CCP that allowed drainage

to occur during testing. Small-scale vane shear tests on FST yielded shear strengths comparable to the undrained strength envelope, which was justified by the considerably lower permeability of FST relative to CCP.

Additional evaluation of small-scale vane shear tests on CCP revealed that rate of rotation and t_d had no influence on measured peak shear strength. This was attributed to the small vane size and high permeability of CCP, which allowed excess pore pressure to dissipate regardless of how fast the material was sheared. Diagenesis was observed to occur in CCP, whereby time-dependent chemical reactions lead to an increase in strength with time. In small-scale vane shear tests on CCP, peak strength was reached after approximately 72 hr. These vane shear tests that accounted for diagenesis (i.e., were allowed to remain under vertical stress for ≥ 72 hr) were found to be most comparable to the drained strength envelope identified via triaxial and direct shear testing. Thus, accurate measures of peak shear strength in CCP must account for diagenesis to occur.

ACKNOWLEDGEMENTS

I would like to thank everybody who contributed in the completion of this work, both directly and indirectly.

The biggest thank you goes to my advisors, Dr. Chris Bareither and Dr. Joe Scalia. Your desire to help me do my best, your continued interest in our project and the many hours you spent reading and editing my thesis are greatly appreciated. Thank you for all the effort you both make in fostering such a fantastic program here at CSU.

To all the people in the geo-group, thank you for making this such a fun and memorable experience. I hope to stay in touch with all of you and look forward to seeing where your careers take you.

To my family and girlfriend, Georgia, thank you for your endless love and support. Thank you for encouraging me to chase my dreams, even if it meant me moving to the other side of the world to pursue them. It is you guys who made me who I am today, and this thesis is as much a reflection of your sacrifice and hard work as it is mine. I love you all. An extra special thank you to my dad, Richard Herweynen, you have been a constant mentor throughout my career and I hope one day I can look back at a career that is even half as successful as yours.

Finally, I am thankful for God and the talents that He has blessed me with. I hope to continue to use them in a meaningful way that makes Him proud.

TABLE OF CONTENTS

LIST OF TABLES

LIST OF FIGURES

LIST OF SYMBOLS

Symbol	Description	Symbol	Description
A, B, Z, C, D	fitting parameters for seepage induced consolidation models	t_d	time delay between vane insertion and beginning rotation
C_c	compression index	t_f	time to failure
c_v	coefficient of consolidation	u_e	excess pore water pressure
d_{max}	maximum particle size	$u_{e,max}$	maximum excess pore water pressure
D_v	diameter of vane	w	gravimetric water content
e	void ratio	$\Delta\sigma_d$	deviator stress
e_i	initial void ratio	$\Delta\sigma_{d,\,max}$	maximum deviator stress
e_f	final void ratio	σ_1'	effective major principal stress
e_0	void ratio at zero effective stress	σ_1	total major principal stress
G_s	specific gravity of solids	σ_3'	effective minor principal stress
H_i	initial specimen height	σ_3	total minor principal stress
H_s	initial height of solids	σ_c'	confining pressure
H_0	specimen height at e_0	σ_h'	effective horizontal stress
H_v	height of vane	σ_h	total horizontal stress
K_f-line	failure line in p'-q space	σ_v'	effective vertical stress
k_s	saturated hydraulic conductivity	σ_v	total vertical stress
LL	liquid limit	δ_h	horizontal deformation
M	maximum torque	δ_v	vertical deformation
p'	mean effective stress	ε_a	axial strain
PI	plasticity index	ϕ'	effective friction angle
PL	plastic limit	ϕ	total friction angle
q	mean shear stress	ϕ_{sc}	secant friction angle
S_u	undrained shear strength	τ	shear stress
$S_{u,v}$	vertical undrained shear strength	τ_p	peak shear strength
$S_{u,h}$	horizontal undrained shear strength	τ_r	residual shear strength
t_c	elapsed time under the final σ_v'		

CHAPTER 1: INTRODUCTION

1.1 Problem Statement

Coal combustion product (CCP) are the by-products from burning coal to generate electricity (EPA, 2018). In 2010, the annual production of CCP worldwide was 780 million Mg (Heidrich, et al., 2013). Despite a growing trend towards natural gas and renewable energy sources, global demand for electricity has continued to increase. This has resulted in an increase in global CCP production (Heidrich, et al., 2013). In 2015, approximately 53% of CCP was beneficially reused or recycled, with predominant end-use as a cementing agent or aggregate in construction applications (ARTBA, 2015). The remaining CCP was disposed in surface impoundments, which presents a considerable cost and risk to utility companies. In 2008 at the Tennessee Valley Authority's (TVA) Kingston Power Plant, a failure of the CCP impoundment lead to the release of 4.2 million m^3 of CCP, which flowed out over the surrounding land and waterways, covering an area of 1.2 km^2 (EPA, 2016). The cost of the spill to the TVA exceeded 1 billion USD (Gang, 2014).

Disposing of CCP in surface impoundments includes numerous geotechnical challenges, and as was observed from the TVA incident, failure can be catastrophic. The flowing nature of the CCP in the TVA failure can in-part be attributed to large volumes of water that are added to CCP to produce a high water content, low solids content slurry, which facilitates pumped transport for disposal into surface impoundments (Evans, et al., 2017). Deposition of CCP at high water contents can result in limited consolidation, resulting in a CCP deposit with high retained moisture and low shear strength. High water content, low shear strength CCP present challenges during closure when equipment need to be safely mobilized onto the impoundment surface for capping and other construction activities. Mobilizing construction equipment onto CCP without sufficient shear strength can lead to bearing capacity failure, which may cause delays in construction, economic losses, injuries, or even loss of life.

At present, the vane shear test is a frequently used in situ test to assess the shear strength of CCP prior to mobilizing construction equipment onto the ponded material surface (Evans, et al., 2017). The vane shear test is inexpensive and fast, and can be performed with a commercially-available, handheld device by field personnel. The vane shear test has been shown to provide reasonable measures of undrained shear strength for clayey materials, as the low permeability of clay does not allow drainage during shear (Blight, 1968). However, CCP typically consists of non-plastic silt-sized particles, making CCP more permeable than clay. Due to the higher permeability, partially-drained conditions can develop during vane shear tests on CCP, whereby some or all of the excess pore pressure developed during shear is able to dissipate. Dissipation of excess pore pressure during shear leads to an increase in effective stress and an overestimation of the undrained shear strength. Limited studies have been completed that compare shear strength measured with vane shear tests to other standard laboratory experiments. Furthermore, most studies have focused on shear strength of clayey materials (e.g., Lefebvre, et al. 1988, Quiros & Young 1988). Continued use of the vane shear test to assess in situ shear strength of CCP requires that vane shear results be compared to standard methods used to measure shear strength to determine if the measured shear strength via vane shear is drained, undrained, or partially drained.

1.2 Research Objectives and Tasks

The objectives of this study were to (i) evaluate the shear strength of CCP via common laboratory experiments, (ii) compare shear strength measured via vane shear to assess drainage conditions present during vane shear in CCP, and (iii) further evaluate drainage conditions during vane shear by testing a material more suitable for conventional vane shear testing. Two materials were used in this study: (i) CCP and (ii) fine-grained synthetic mine tailing (FST). The FST was selected as this material contained approximately 40% clay-sized particles by mass. The clay

content of FST yielded lower permeability, which was more suitable for conventional vane shear testing, where the undrained strength is measured.

The following research tasks were completed as part of this study:

1. Classified CCP using standard geotechnical characterization tests, including particle-size distribution, specific gravity, and Atterberg limits.

2. Developed specimen preparation procedures for CCP slurries to create uniform, repeatable specimens for shear testing.

3. Developed laboratory apparatuses to support vane shear testing with a small-scale vane (diameter = 12.5 mm and height = 25 mm) and large-scale vane (diameter = 25 mm and height = 50 mm).

4. Evaluated compressibility and hydraulic properties of CCP.

5. Evaluated shear strength of CCP and FST.

6. Evaluated the effects of vane shear test variables on CCP (e.g., rate of rotation, vane insertion effects, etc.).

7. Compared shear strength properties measured using vane shear to drained and undrained strength envelopes for CCP and FST.

Seepage induced consolidation testing (SICT) was used to measure the compressibility and hydraulic properties of CCP. Drained and undrained shear strength of CCP was measured by consolidated undrained (CU) triaxial compression. Shear strength of CCP was also measured using direct shear, and small-scale and large-scale vane shear. Vane shear test variables were evaluated on CCP using small-scale vane shear tests. The high permeability of CCP meant that it was anticipated that partially-drained or drained conditions would develop during shear, leading to an overestimate of the undrained strength.

Shear strength of FST was evaluated in small-scale vane shear. These tests were conducted to further assess the drainage conditions during vane shear, using a material more suited to measuring undrained shear strength by vane shear testing. The low permeability of FST

meant that the vane shear was anticipated to yield more accurate measures of undrained shear

strength relative to CCP.

CHAPTER 2: BACKGROUND

2.1 Properties of CCP

The characteristics and engineering properties of CCP have been assessed extensively (EPRI, 2012). Coal combustion products are mainly composed of aluminum silicates, with smaller amounts of iron and calcium oxides (Fe_2O_3 and CaO) (EPRI, 2012). Particle-size distributions show that CCP is predominantly composed of silt-sized particles, with some sand- and clay-sized particles. Scanning electron microscope studies have shown CCP particles to be generally spherical in shape (EPRI, 2012).

A study by the Electric Power Research Institute (EPRI, 2012) provided a compilation of engineering properties of CCP from a number of past studies. In general, CCP is designated as non-plastic and typically classified as low plasticity silt (ML). The specific gravity of solids (G_s) for CCP has a much larger range than natural soils, ranging between 2.2 and 3.3 for CCP produced in the U.S. The saturated hydraulic conductivity (k_s) of CCP typically ranges between 1 x 10^{-5} to 1 x 10^{-7} m/s, and in a limited number of studies was shown to be independent of vertical effective stress (σ_v'). This range of k_s is higher than what would be expected for CCP based solely on particle size (EPRI, 2012). Consolidation data for CCP illustrate CCP to have low compressibility. Shear strength measured using various laboratory methods revealed a broad range of effective friction angles (ϕ') for CCP, from 22° to 47°. The deposition environment of CCP (i.e., loosely deposited as a slurry) can lead to highly contractive behavior during undrained loading, making CCP susceptible to rapid loss of shear strength and potentially liquefaction.

Coal combustion products have been shown to exhibit time-dependent engineering properties, such as consolidation and shear strength. Diagenesis is a defined change in mineralogy due to chemical reactions that occur following disposal of CCP into a surface impoundment (McCarthy, et al., 1999). Changes in mineralogy can lead to an increase in stiffness

over time, which may lead to higher shear strength of ponded CCP. Disturbance of the ponded CCP may eliminate the beneficial strength gain due to diagenesis. EPRI (2012) also reported that a stiffer CCP structure developed as a result of diagenesis may hinder consolidation and preserve an open, brittle structure. Subsequent loading of CCP that has undergone diagenesis can lead to collapse of the structure.

2.2 Undrained Shear Behavior of Low-Plasticity Silts

The shear behavior of non-plastic silt (e.g., CCP) differs from the shear behavior of clay and sand. Typically, sand and clay tend to contract when prepared loose or normally consolidated, and dilate when prepared dense or overconsolidated. This tendency to either dilate or contract controls the excess pore pressure that develops during undrained shear. A contractive material will develop positive excess pore pressure (u_e), which reduces the effective stress and can lead to strain-softening behavior. A dilative material will develop negative u_e, which increases the effective stress and can lead to strain-hardening behavior. Unlike sand and clay, non-plastic silts can exhibit dilative behavior regardless of whether the silt is normally consolidated or overconsolidated (Brandon, et al., 2006).

The dilative behavior of non-plastic silt can make consolidated undrained (CU) triaxial compression testing challenging. Initially saturated specimens may become unsaturated due to cavitation, which occurs when large negative u_e develops during undrained shear. Backpressure saturation is used to avoid this phenomenon and to help maintain dissolved air in solution. However, cavitation can occur as u_e becomes increasingly negative and exceeds the backpressure, allowing air to come back out of solution. Brandon et al. (2006) recommended using higher-than-normal backpressure to maintain saturation when shearing non-plastic silt undrained, which can allow full development of negative u_e without causing cavitation.

The negative u_e developed during undrained shear of dilative silts can also lead to difficulties when trying to establish a failure criterion. As axial strain increases during CU

compression, u_e can become increasingly negative, which leads to strain-hardening behavior and increasing deviator stress ($\Delta\sigma_d$) due to a continuous increase in effective stress (σ'). This behavior has been shown to continue to axial strain ≥ 30%. In this case, a typical failure criterion based on the maximum $\Delta\sigma_d$ may not make sense, as large axial strain must occur before a peak $\Delta\sigma_d$ is achieved. Furthermore, the maximum $\Delta\sigma_d$ relies on the development of negative u_e. Brandon et al. (2006) evaluated the shear behavior and shear strength of silty soils and identified six possible failure criteria: (1) maximum deviator stress, $\Delta\sigma_{d,max}$; (2) maximum principal effective stress ratio, $(\sigma_1'/\sigma_3')_{max}$; (3) maximum excess pore water pressure, $u_{e,max}$; (4) Shear-induced excess pore water pressure equal to zero, ($u_e = 0$); (5) effective stress path reaches the failure line in p'-q space (K_f-line); and (6) limiting axial strain (e.g., ε_a = 5 or 10 %).

Brandon et al. (2006) showed that the failure criteria of $u_e = 0$ yielded the most consistent results because this ensured that no reliance was placed on strength that results from negative changes in u_e. The six failure criteria have also been evaluated by Wang and Luna (2012) and Jehring and Bareither (2016), whereby the latter study considered all possible interpretations of failure for different mine waste materials. Jehring and Bareither (2016) identified three methods that were broadly applicable and yielded the smallest bias (i.e., $\Delta\sigma_{d,max}$, K_f-line, and ε_a = 15%).

2.3 Vane Shear Test

The in situ shear strength of CCP in surface impoundments is frequently measured using the vane shear test or cone penetration test (CPT). Vane shear has the advantages of being inexpensive, rapid, and performed with a simple, handheld device. On the other hand, cone penetration requires specialized equipment (e.g., piezocones) and post-processing of data to generate estimates of shear strength (Robertson, 2009). Therefore, vane shear is the in situ strength test commonly used by contractors to assess shear strength of ponded CCP (Evans, et al., 2017).

2.3.1 General Characteristics

Vane shear is the most widely used method to directly measure in situ undrained shear strength of soft clays (Chandler, 1988). Other in situ test methods, such as cone penetration, are not direct measures and rely on correlations to estimate undrained shear strength. The field vane was developed in Sweden in 1919, and has since progressed into the modern vane shear test based on work by Carlsson (1948), Skempton (1948), and Cadling and Odenstad (1948).

A standard field vane consists of four blades set at right-angles to one another, with a height-to-diameter ratio of 2:1. The size of field vanes vary, but the most widely used dimensions are height (H_v) = 130 mm and diameter (D_v) = 65 mm (Chandler, 1988). The vane is attached to the end of a rod (or series of rods depending on depth) that can be pushed into the ground from the surface or bottom of a borehole. A typical vane can be rotated manually or by a motor. As the vane rotates in the soil, torque is measured and the maximum torque is correlated to the undrained shear strength.

The conventional equation for vane shear is

$$S_u = \frac{6M}{7\pi D_v^3}$$

(2.1)

where S_u is undrained shear strength and M the maximum measured torque. The assumed failure surface and shear stress distribution for vane shear is shown in Fig. 2.1. A cylindrical failure surface is assumed with a uniform shear stress distribution on both the vertical and horizontal surfaces. Several investigations have shown that this assumed stress distribution is conservative and leads to low values of S_u (Donald, et al., 1977; Menzies & Merrifield, 1980). Other assumptions incorporated into vane shear testing include an (i) isotropic shear strength (i.e., equivalent vertical and horizontal strength, $S_{u,v} = S_{u,h}$) and (ii) undrained conditions are maintained during the entire test.

2.3.2 Vane Shear Test in Low-Plasticity Silts

Achieving undrained conditions during vane shear is critical to accurately estimate S_u (Blight, 1968, Chandler, 1988, Morris & Williams, 2000). In contractive materials (e.g., normally consolidated clays), positive u_e is generated during vane insertion and rotation. If drainage is allowed to occur during vane shear, dissipation of positive u_e can lead to consolidation and subsequent increase in effective stress and shear strength. Thus, partially-drained conditions in contractive materials yield an overestimation of S_u. The two variables which have been shown to influence the degree of u_e dissipation in vane shear are (i) the rate of vane rotation and (ii) delay between vane insertion and beginning shearing. Standard vane shear test methods were developed for soft clays and have been shown to be unsuitable for measuring S_u in silty materials (Reid, 2016).

Blight (1968) proposed a relationship between time to failure (t_f) and degree of drainage, which is shown in Fig. 2.2. Degree of drainage refers to the amount of u_e that dissipates during shear. Blight assumed a spherical area of influence around the vane, with a drainage path for dissipation of u_e equal to D_v. The t_f was defined as the time between initiating rotation and reaching peak shear strength (τ_p) that corresponded with the maximum torque (Eq. 2.1). Blight (1968) suggested that to ensure undrained conditions were maintained during vane shear, a t_f that resulted in a degree of drainage less than 10% should be targeted. Therefore, given two materials with different permeabilities (e.g. a silt and a clay) but the same time to failure (e.g. 2 minutes), vastly different degrees of drainage would be expected. A time to failure of 2 minutes may maintain undrained conditions in a clayey material, but partially-drained conditions may develop for a silty material due to higher permeability. Morris and Williams (2000) proposed a revision to Blight's model and suggested t_f should instead be measured from the beginning of vane insertion. They showed that most u_e was generated by vane insertion, rather than during shear.

Reid (2016) conducted a series of vane shear tests in a mine tailings facility containing predominantly silt-sized tailings. Tests were conducted at a standard rate of rotation of 12°/min,

as well as 90°/min and 240°/min. The measured τ_p from vane shear tests were compared to S_u measured using laboratory direct simple shear tests and in situ cone penetration. Results demonstrated that faster rotation rates led to undrained conditions, and the measured τ_p agreed well with S_u measured via direct simple shear tests and CPT. At the standard rotation rate of 12°/min, partially-drained conditions developed within the silty mine tailings and the measured τ_p was higher than S_u.
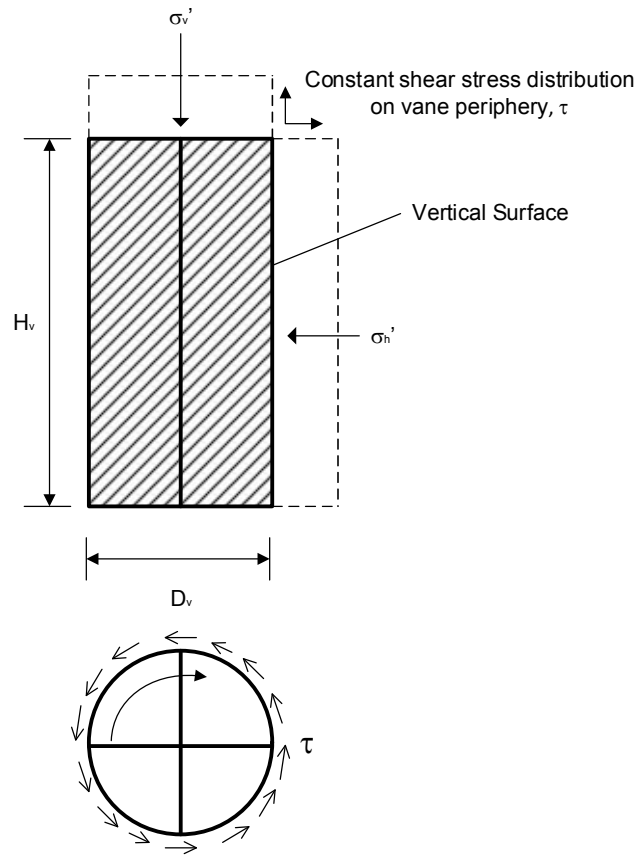
Fig. 2.1. Conventional shear stress distribution around vane periphery.
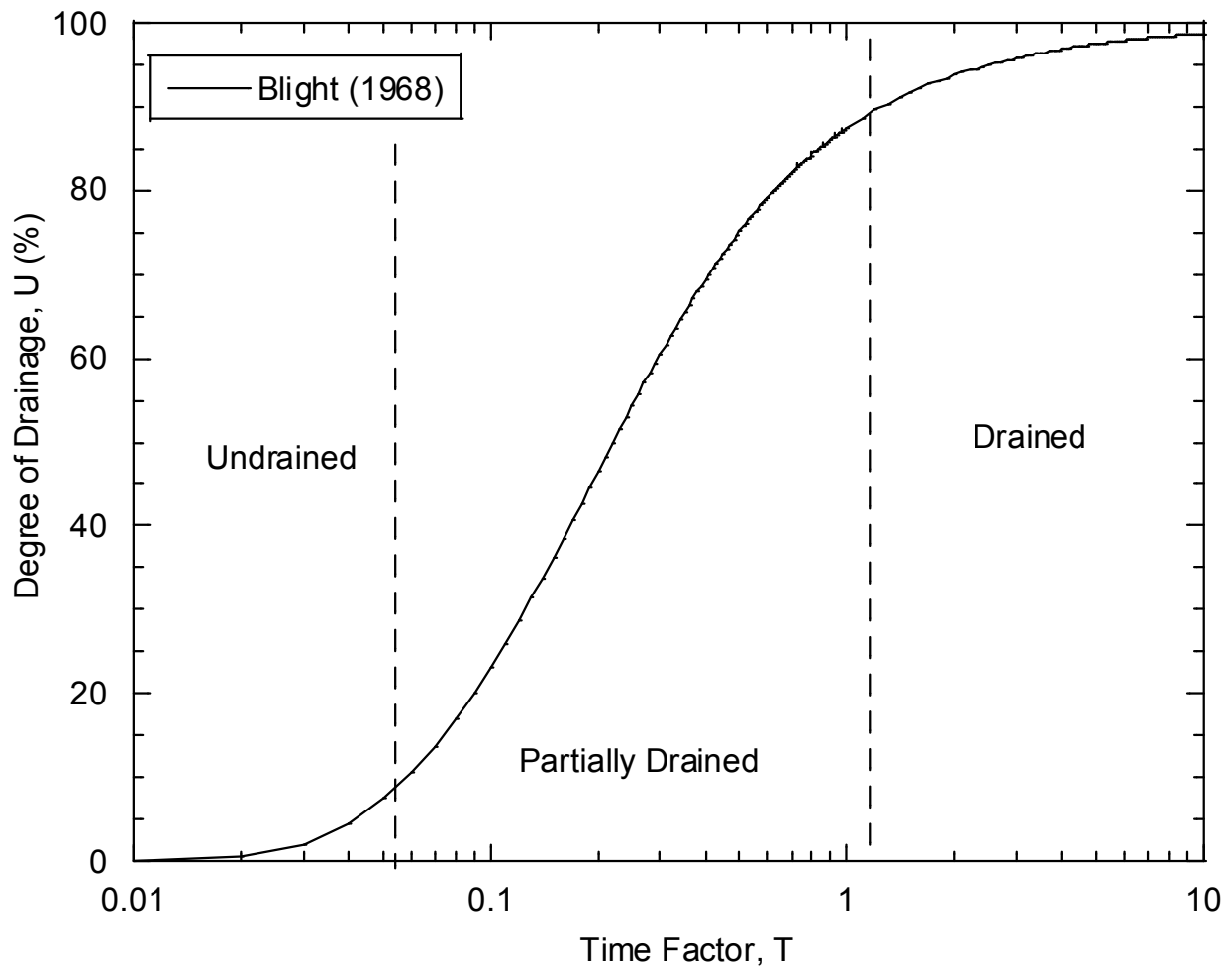
Fig. 2.2. Relationship of degree of drainage versus time to failure for vane shear tests *(Blight, 1968)*.

CHAPTER 3: MATERIALS AND METHODS

This study included two materials: CCP and fine synthetic tailings (FST). The CCP samples were provided by Remedial Construction Services (RECON) from an unnamed evaporation pond in the Eastern U.S. The FST was a blend of commercially-available materials used to replicate the particle-size distribution (PSD) of actual mine tailings. The blend targeted the finer-grained boundary of a compilation of PSDs of actual mine tailings from literature (Hamade, 2017). The FST prepared for this study included 40% silica powder, primarily containing silt-size particles (U.S Silica, Maryland, U.S.A.), and 60% kaolin clay (Thiele Kaolin Company, U.S.A.).

3.1 CCP

The PSD curves for five CCP samples that represented different sampling depths within a CCP impoundment are shown in Fig. 3.1. Samples were collected from the impoundment surface to depths of approximately 2 m, and a mechanical sieve and hydrometer were conducted on each sample following ASTM D 6913 and ASTM D 7928. The CCP samples were predominantly silt, with the sand-sized fraction ranging from 8% to 47% (> 0.075 mm), and all samples had less than 2% clay-sized particles (< 0.002 mm) by mass. In general, the PSDs were similar and a single composite material was created for laboratory testing (Fig. 3.1); to prepare the composite material, samples from all depths were air-dried and manually combined together to form a single, homogenized sample.

Geotechnical properties for the composite CCP sample are tabulated in Table 3.1. Atterberg limits were determined using the fall cone test for liquid limit (*LL*) following BS 1377 and the plastic limit (*PL*) was determined following ASTM D 4318. The *LL* was 41 and no *PL* could be identified such that the material was classified as non-plastic. The CCP classified as low plasticity silt (ML) according to the Unified Soil Classification System (USCS). Specific gravity (G_s) was

13

determined using the water pycnometer method described in ASTM D 854; the G_s was 2.35. Geotechnical characteristics of the CCP used in this study were comparable to characteristics reported in a comprehensive compilation by EPRI (EPRI, 2012).

3.2 Fine Synthetic Tailings

Soil classification data for FST was adopted from Hamade (2017). The PSD curve for FST is shown in Fig. 3.2 and the geotechnical characteristics are in Table 3.1. The FST was a fine-grained material, with 42% clay-sized particles (< 0.002 mm) by mass. Fine synthetic tailings classified as low plasticity clay (CL) according to the USCS with LL = 37 and plasticity index *(PI)* = 15%. Specific gravity for FST was 2.63.

PSDs of FST and the composite CCP are compared in Fig. 3.2. Both are predominantly fine-grained materials, with the CCP having some coarser particles. The FST has a higher percentage of clay-sized particles compared to the CCP.

3.3 Slurry Preparation and Void Ratio Calculation

Specimens for all experiments conducted on CCP and FST in this study were prepared via slurry deposition. The CCP and FST slurries were prepared by mixing tap water and air-dried material. Slurries for triaxial testing were prepared using de-aired water instead of standard tap water to accelerate specimen saturation. The CCP slurry was prepared at a solids content of 57%, which equated to a gravimetric water content of 75%. The FST was prepared at a solids content of 44%, which equated to a gravimetric water content of 127%. Both slurries were prepared at water contents that exceeded the LL and were at a consistency that could easily be poured to create test specimens. Slurries were thoroughly mixed by hand using a spatula or stirring rod to create uniform slurries for all test specimens.

Since diagenesis is known to occur in CCP, where possible a minimum of 48 hours was maintained between preparing the sample and beginning testing. By doing this, any strength gain

with time due to diagenesis was consistently accounted for in all tests. Importantly, CCP samples were only used once and were not reused in future tests. The exception was in the LS-VS tests which required large amounts of material, so CCP material was reused.

The initial water content (*w*) of the slurry was measured to confirm the consistency of a given slurry. Using the initial *w* and assuming the specimen was saturated, an initial void ratio (*e*) was calculated using Eq. 3.1.

$$e = w.G_s \tag{3.1}$$

Similarly, after specimen consolidation was complete for a given test specimen, the final void ratio (*e$_f$*) was determined by measuring the final water content after testing and assuming the specimen remained saturated.

3.4 Seepage Induced Consolidation Testing

Seepage induced consolidation testing was conducted on CCP to determine compressibility and hydraulic conductivity. A schematic of the SICT apparatus is shown in Fig. 3.3 (Tian, 2017). The apparatus includes a 152-mm diameter specimen cell, flow pump capable of controlling flow rate over a range of permeability applicable to fine-grained geomaterials, vertical loading piston with load cell, a Mariotte bottle to create a constant head on top of the specimen, and top and bottom pressure transducers for measuring pore pressure. Details of the design, calibration, and assessment of the SICT are in Tian (2017).

The SICT procedure consisted of three steps. In the first step, the void ratio at zero effective stress (*e$_0$*) was determined. This corresponded to the void ratio at the end of sedimentation and onset of consolidation. The *e$_0$* was determined via depositing a known mass of slurry into the specimen cell to an initial thickness of approximately 80 mm. The slurry was allowed to settle and supernatant water was subsequently removed. The final thickness of the sedimented slurry was measured via a measuring tape with millimeter increments affixed to the outside of the specimen cell. The average *w* and *e$_0$* were computed assuming 100% saturation.

Following self-weight consolidation, filter paper and a porous plastic disk were placed on top of the specimen. Two linear potentiometers were immediately set in-contact with the plastic disk to monitor deformation. The linear potentiometers induced σ_v' = 0.28 kPa on the specimen. The second step began immediately after setting the potentiometers in place.

In the second step, the flow pump was used to create downward seepage within the slurry and induce consolidation. A constant flow rate was imposed on the specimen until steady-state was achieved, which was identified as a constant pressure difference across the specimen ($\pm$ 0.1 kPa). The pressure difference was computed via pressure transducers at the top and bottom of the specimen. Steady-state was also confirmed as no subsequent change in vertical deformation measured with two linear potentiometers (Fig. 3.3). A steady-state e and k_s were calculated for each imposed flow rate. The k_s was computed by Darcy's Law using the pressure difference and specimen height at steady-state. Furthermore, the seepage force varied across the specimen at steady-state conditions, which in turn yielded decreasing e with depth in the specimen from the top surface. Void ratio at the mid-depth was adopted herein as a measure of the average e of the specimen at steady-state. This second step was repeated for at least three unique flow rates to obtain e and k_s that corresponded to three different σ_v'.

The third step involved vertical load application via a pneumatic air cylinder connected to a load piston (Fig. 3.3). A load platen was added to the top of the specimen prior to applying the vertical load. The load platen applied σ_v' = 0.30 kPa. The third step was initiated once sufficient consolidation was achieved during the seepage phase ($\sigma_v' \approx 5$ kPa), and the first load applied via the air cylinder targeted $\sigma_v' \approx 10$ kPa. Steady-state consolidation during each vertical load increment was verified via measurements of pore pressure and vertical displacement. The e at steady-state was computed directly from mass-volume relationships assuming that σ_v' applied via the load piston was transferred equally with depth in the specimen and e was constant throughout the specimen. The k_s at steady-state was determined via applying a small flow rate that would not

16

induce further measurable consolidation, but was large enough to induce a measureable pressure difference across the specimen to compute k_s. This third step was repeated until a final, target σ_v' was reached. At the end of an experiment, the specimen was removed to measure the final w and compute a final e.

Data analysis for the SICTs was performed based on the theory described by Liu and Znidarčić (1991) with implementation in Microsoft Excel. Liu and Znidarčić (1991) proposed the following two relationships to define the compressibility (e-σ') and hydraulic conductivity (k_s-e) relationships for a SICT test:

$$e = A(\sigma' + Z)^B \tag{3.2}$$

$$k_s = C.e^D \tag{3.3}$$

where *A*, *B*, *Z*, *C*, and *D* are fitting parameters. These fitting parameters were determined via the Solver function in Excel, which was programmed to minimize the sum of squared residuals between the measured data and predicted e-σ' and e-k_s relationships.

3.5 Triaxial Compression Testing

Consolidated undrained (CU) triaxial compression tests were conducted on CCP specimens prepared via slurry deposition following the method described by Jehring and Bareither (2016). A schematic of the specimen preparation apparatus is shown in Fig. 3.4 (Jehring & Bareither, 2016). The slurry was poured into a 38-mm diameter by 100-mm tall split mold, lined with a 0.25-mm-thick latex membrane. Conventional 38-mm diameter triaxial specimens were used since the maximum particle diameter (d_{max}) for CCP was $\leq$ 2 mm. A 70-mm-tall extension collar was added to the top of the split mold to increase the height such that a sufficient height to diameter ratio of the specimen was maintained after consolidation.

A thin paper mold was placed around the outside of the membrane prior to assembling the split mold and depositing the slurry. The paper mold was held together with tape and provided

stability to the test specimen following removal of the split mold. Once water was added to the triaxial cell to apply the confining pressure, the paper lost strength and tape lost adhesion such that the paper mold fell apart prior to shearing.

Triaxial test specimens were consolidated via vertical stress application prior to removing the split mold. After consolidating under the target σ_v', specimens were then subjected to an isotropic, effective confining pressure (σ_c') in the triaxial cell. Consolidation under vertical stress was used to simulate the anticipated stress condition within a CCP impoundment. Slurry deposited specimens were initially allowed to settle and consolidate under self-weight for at least three hours. Subsequently, dead weight was applied to the loading plate (Fig. 3.4) to reach target σ_v' of 10, 20, 50, and 100 kPa. The range of stress was selected to be representative of a typical CCP impoundment. For stresses higher than 10 kPa, the vertical load was applied incrementally, with a load increment ratio of unity (i.e., load was doubled each time). Vertical deformation was monitored during each σ_v' such that consolidation was completed for each load increment. Complete consolidation was assumed when no further deformation was observed. A coefficient of consolidation (c_v) was also calculated for the CCP using relationships of settlement versus time developed from the SICT. Based on the calculated c_v, a time increment of two hours was sufficient between each load increment for complete consolidation.

Consolidated undrained triaxial compression tests were conducted in accordance with ASTM D 4767. The target σ_c' were 10, 20, 50 and 100 kPa, which were the same as the applied σ_v' during specimen preparation. All CU specimens were back-pressure saturated to achieve a B-value of ≥ 0.95. Shearing was conducted via axial loading at an axial strain (ε_a) rate of 1 %/hr to a maximum $\varepsilon_a \geq 20\%$. The axial strain rate was determined via ASTM D 4767 to promote pore pressure equilibration throughout the specimen during shear. The specimen void ratio after consolidation under the target σ_c' and during undrained shear was determined via Eq. 3.1 using the final measured w.

Measurements of vertical load, vertical displacement, cell pressure, and pore water pressure were collected by a data acquisition system (CU Triaxial Mode, GeoTac) connected to a PC. Axial load was measured using an 8900 ± 0.4 N load cell (Artech Industries, Inc.) and axial displacement was measured with a 50 ± 0.003 mm displacement transducer (Novotechnik). Cell pressure and pore pressure were monitored with pressure transducers (GeoTac, 1378 ± 0.07 kPa; ELE International, Ltd., 700 ± 0.07 kPa).

3.6 Direct Shear Testing

Direct shear tests were conducted under consolidated drained conditions on CCP specimens prepared via slurry deposition. Direct shear testing was conducted under target σ_v' between 30 and 100 kPa. Slurry was poured into a standard 63-mm diameter by 33-mm tall circular shear box. A 3-mm-thick porous plastic disc and filter paper were placed at the bottom of the shear box and on top of the test specimen.

Specimens were consolidated within the shear box in the direct shear apparatus via vertical loading using a 10-to-1 moment arm. Specimens were initially allowed to consolidate under self-weight for at least three hours and subsequently were loaded incrementally to the target σ_v'. A load increment ratio of unity was used for preparing all test specimens and loads were applied every two hours. This time interval coincided with complete consolidation under a given load increment based on time-rate consolidation properties of the CCP.

Direct shear testing was conducted in accordance with ASTM D 3080 using an ELE International direct shear apparatus. Shear stress was measured using a 2220 ± 0.4 N load cell (Interface Inc.), vertical and horizontal displacement was measured with linear potentiometers (Novotechnik, 25 ± 0.003 mm; Novotechnik, 50 ± 0.003 mm). Data acquisition was conducted using LabView and a National Instruments USB data acquisition module. All tests were sheared to a horizontal displacement of at least 15% the specimen diameter at a displacement rate of 0.08

mm/min. This horizontal displacement rate was conservatively selected based on ASTM D 3080 such that drained conditions persisted throughout the specimen during shear.

Consolidation was monitored via a linear potentiometer. The e after shear was determined by taking the w of the specimen (Eq. 3.1). Vertical deformation data was used to back calculate the e prior to shearing.

3.7 Vane Shear Testing

Vane shear testing was conducted in specially-designed laboratory cells that allowed consolidation and shearing under a target σ_v'. Two different sized cells were constructed: the small-scale vane shear (SS-VS) apparatus was 63 mm in diameter and the large-scale vane shear (LS-VS) apparatus was 292 mm in diameter. All CCP and FST specimens tested in vane shear were prepared from slurry such that all specimens were considered normally consolidated when sheared. Vane shear testing was conducted in accordance with ASTM D 4648.

3.7.1 Small-Scale Vane Testing

3.7.1.1 Apparatus

A schematic of the SS-VS apparatus is shown in Fig. 3.5. The cell consisted of an acrylic cylinder (6-mm wall thickness) with an inside diameter of 63 mm and height of 90 mm. The cylinder was attached to a bottom acrylic pedestal that was bolted to a steel base plate. A bead of silicon was used between the cylinder, steel base plate, and bottom pedestal to create a watertight seal. A drain line was machined into the side-wall of the cylinder at the bottom of the cell to allow drainage and measure pore pressure at the base of the specimen. A porous plastic disk and filter paper were placed at the base of the cell to prevent clogging of the drain line.

A dead-weight loading system consisting of a top acrylic load platen placed on the specimen, a circular riser tube, and a square acrylic plate attached to the riser tube (Fig. 3.5), were used. Filter paper was placed between the specimen surface and top load platen. Holes in

the center of top load platen, load plate, and dead weights allowed the vane to be inserted into the specimen without removing the vertical load. A small piece of aluminum foil was attached to the base of the top load platen that spanned the center hole. The foil was used to prevent slurry from puncturing the filter paper and squeezing out of the hole in the load platen during consolidation. The vane could easily be pushed through the aluminum foil and filter paper for testing.

Vertical displacement of the top load platen was measured using a dial gauge (Fig. 3.5) and a measuring tape adhered to the side of the cell. Pore pressure at the bottom of the specimen was monitored using a manometer. An ELE International laboratory vane apparatus was used to measure shear strength. Shear stress was applied to a given test specimen through a 12.7-mm-diameter x 25.4-mm-tall vane using one of four calibrated springs. The four springs each supported a different range of available torques that were calibrated to shear strength. A small electric DC motor was retrofit to the vane apparatus to provide a constant rate of rotation of the vane. Three interchangeable 12-V DC motors were used to allow a range of vane rotation rates from 5 °/min to 300 °/min.

3.7.1.2 Procedure

Small-scale vane shear tests were conducted under σ_v' ranging from 17 to 94 kPa. The CCP and FST slurries were poured into the specimen cell and allowed to consolidate under self-weight. An extension collar was used when testing the FST to account for greater compressibility. After self-weight consolidation was complete, filter paper was placed on the specimen surface, the vertical loading system was put in place, and dead weights were incrementally added to the loading plate to reach the target σ_v'. Consolidation was monitored via pore pressure at the base of the specimen and vertical deformation, and was determined to be complete at each increment prior to subsequent loading. Complete consolidation was reached once deformation had stopped

and excess pore pressure had dissipated. The extension collar used when preparing FST specimens was removed after achieving $\sigma_v' = 10$ kPa and the specimen was trimmed to the top of the cell; consolidation was then continued to the target σ_v'. For a typical SS-VS test on CCP, the specimen remained in the cell for 24 hr to ensure that any time-dependent strength gain due to diagenesis was consistent.

The SS-VS test was conducted in accordance with ASTM D 4648. The vane was inserted into a specimen to a depth such that the top of the vane was at least one vane height (25.4-mm) below the specimen surface. The standard SS-VS test procedure was as follows: (1) specimens were consolidated under the target σ_v' for 24 hr; (2) 1 min was allowed to elapse between inserting the vane and beginning rotation; (3) shearing was conducted at a constant rotation rate of 60 °/min until a peak torque was measured; (4) the vane was rapidly rotated at least five revolutions and residual shear strength was measured; and (5) a final height of the specimen was recorded, the average w was determined on the specimen after testing, and a final e was computed ($e = w \cdot G_s$ for 100% saturation).

Aside from the standard test procedure noted previously, the following test variables were evaluated for CCP: (i) elapsed time under the final σ_v' (t_c); (ii) rate of vane rotation; and (iii) time delay between vane insertion and beginning rotation (t_d). The t_c was varied between one hour and seven days. Rate of rotation was varied between 5 °/min and 300 °/min. The t_d was varied between 0 and 60 min. These variables were evaluated to assess the influence of each on τ_p and to assess what approach yielded drained or undrained shear strength via comparison to triaxial and direct shear measurements.

3.7.2 Large-Scale Vane Shear Testing

3.7.2.1 Apparatus

Cross-section and plan-view schematics of the LS-VS apparatus are shown in Fig. 3.6. The apparatus was developed with the similar objective as the SS-VS, whereby specimens could be consolidated and sheared under a target σ_v' without removing the applied load. The cell consisted of an acrylic cylinder with an inside diameter of 292 mm (6-mm wall thickness) and height of 610 mm. The cylinder was attached to a steel base plate using silicon caulk to provide a watertight seal. A hole was tapped into the side-wall of the cylinder at the bottom of the cell to allow drainage. Thus, all specimens were doubly-drained during vertical loading to decrease the time required for consolidation. A flexible tube connected to the bottom drainage outlet was positioned at an equal height to the top of the specimen such that seepage did not develop. A non-woven geotextile was used as a filter layer at the base to prevent material from migrating into the drainage line.

A loading frame was fabricated with a 9-to-1 moment arm to facilitate testing at the same target σ_v' as in the SS-VS. The load frame was constructed from pre-fabricated square steel tubes that were 50 mm x 50 mm in cross section (Fig. 3.6). Buckets of sand were hung from the end of the 1.8-m long moment arm, which was transferred to the specimen at a 9-to-1 ratio. A 20.5 kg counterweight was used to offset the weight of the moment arm. Vertical load was transferred to the specimen through four 9-mm-diameter steel rods positioned on the upper load platen. The load platen was a 291.5-mm-diameter by 12-mm-thick plastic plate that had a 54-mm-diameter hole in the center to allow the vane to be inserted into the specimen. A thin non-woven geotextile with a 54-mm slit was used as a filter layer between the surface of the specimen and load platen. Aluminum foil was placed over the hole in the load platen in a similar manner to the SS-VS. This method was used to prevent squeezing out of material during consolidation. The vane could easily be pushed through the aluminum foil and filter paper for testing. Vertical displacement was

monitored during consolidation using an adhesive-backed measuring tape affixed to the side of the cell.

A Humboldt handheld field vane was used to measure shear strength. Shear stress was applied to a test specimen through a 25.4-mm-diameter by 50.8-mm-tall vane. The Humboldt field vane used in this study allowed a shear stress between 0 and 65 kPa to be measured with an accuracy of $\pm$ 10%. The moment arm was calibrated using a 2.2-kN load cell set in place of the specimen. The load generated with the moment was verified to be transferred at a 9-to-1 ratio from the hanging bucket of sand to the test specimen.

3.7.2.2 Procedure

Large-scale vane shear tests were only conducted on CCP. Slurries were poured into the specimen cell and allowed to consolidate under self-weight. After self-weight consolidation was complete, the top filter layer and load plate were set in place on the surface of the specimen. An initial σ_v' of approximately 1 kPa was applied to a test specimen via directly placing a sand-filled (3.94 L) bucket on the load plate. All subsequent σ_v' were applied via the moment arm. The mass of sand was incrementally increased within the hanging buckets by known amounts and consolidation was allowed to complete under each increment to the target σ_v'. Consolidation was monitored via a ruler on the side of the cell and loads were added approximately every 24 hr. For a typical test, the CCP specimen remained in the cell for five days prior to testing.

The LS-VS test was conducted in accordance with ASTM D 2573. The vane was inserted to approximately the mid-depth of the specimen. The specimen height was sufficient such that the top of the vane was deeper than one vane height (50.8 mm) below the sample surface. A five minute delay was maintained between the vane reaching the final position for shearing and beginning vane rotation. The vane used in the LS-VS tests was handheld, and was rotated "as slow as possible" as per instructions provided by the manufacturer. The achieved rate of rotation

was approximately 10 °/min, which was a slow as possible. ASTM D 2573 suggests a rate of rotation of 6 °/min, with permissible variations in the range of 3 ° to 7 °/min. Peak shear strength was measured, and the vane was then rapidly rotated at least five revolutions and residual shear strength was measured. A final height of the specimen was recorded, the average w was determined via sampled material, and the final e computed assuming 100% saturation.

Large-scale vane shear tests were conducted on CCP at σ_v' = 40 and 90 kPa. A total of two tests were conducted for each σ_v' to demonstrate repeatability of the sample preparation and test procedure, as well as to compare to shear strength measured via SS-VS, direct shear, and CU triaxial compression.

Table 3.1. Summary of material physical characteristics and classification.

Material	LL (%)	PI (%)	USCS	d_{max}	Sand Content (%)	Silt Content (%)	Clay Content (%)	G_s
Fly Ash	41	-	ML	2.00	15	83	2	2.35
FST	37	15	CL	0.05	0	58	42	2.63

Notes: LL = liquid limit; PI = plasticity index; USCS = Unified Soil Classification System; d_{max} = maximum particle size; G_s = specific gravity of solids.
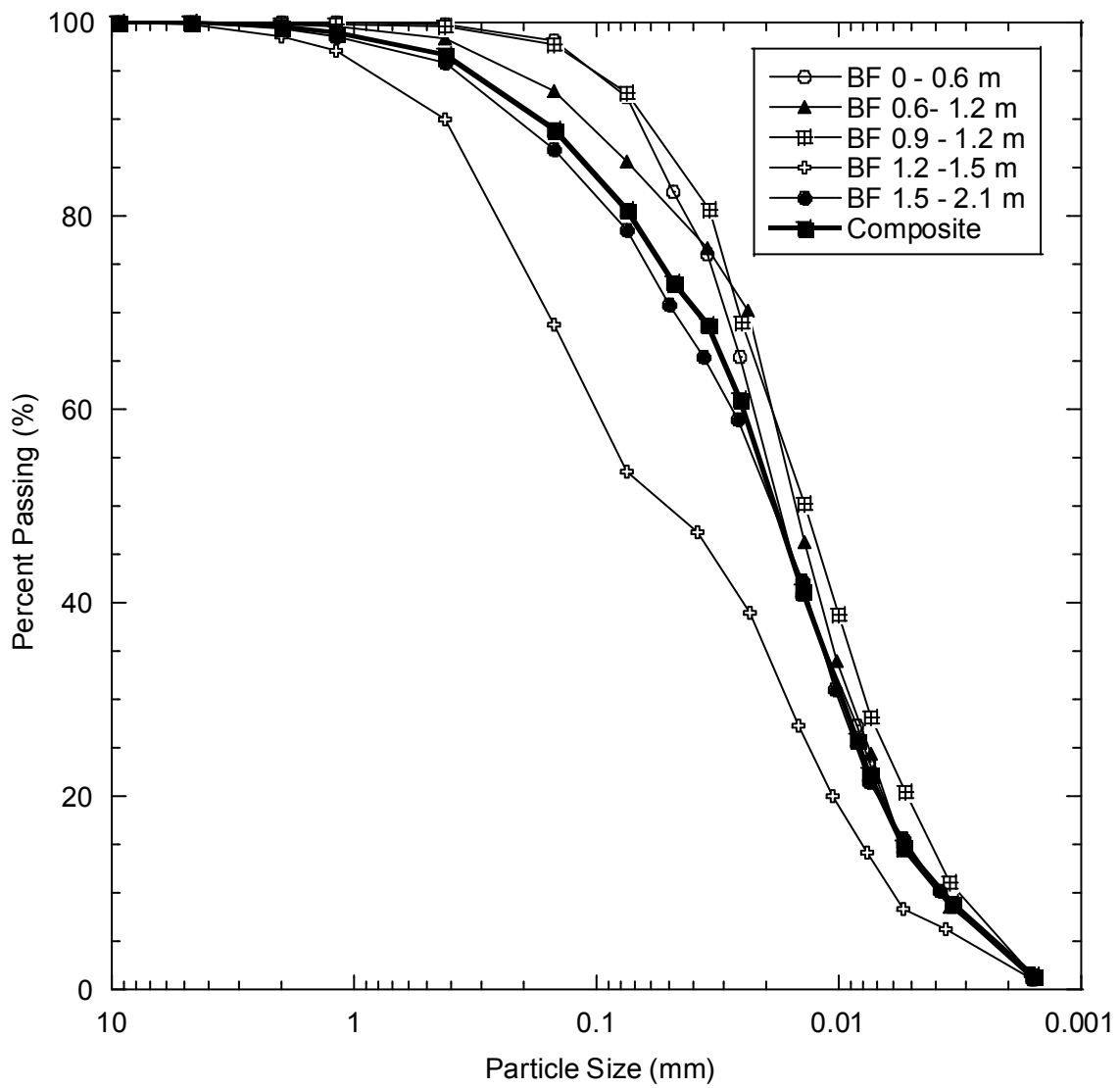
Fig. 3.1. Particle size distribution of CCP samples provided by RECON for this study.
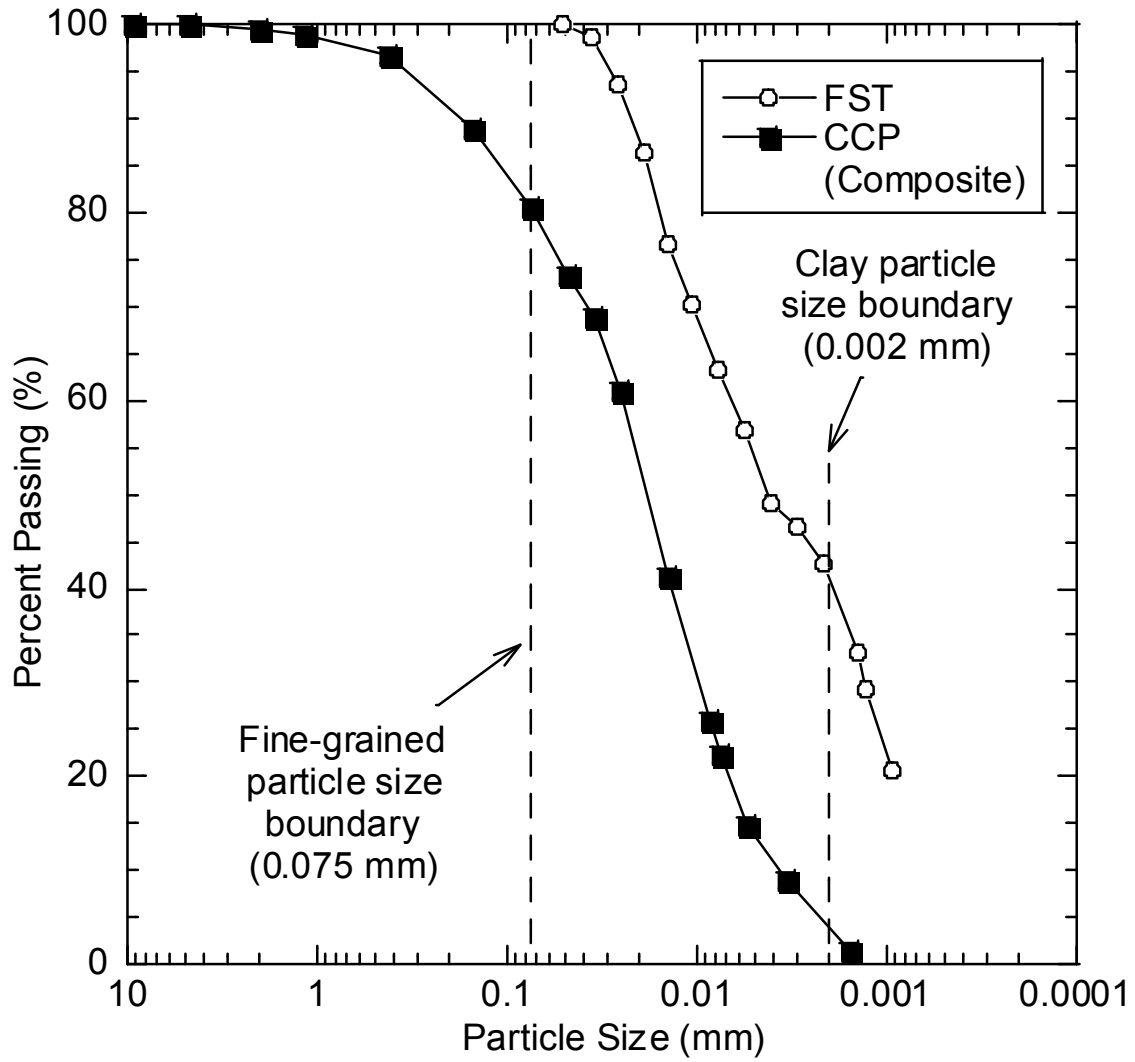
Fig. 3.2. Particle size distribution for fine synthetic tailings (FST). CCP composite PSD shown for comparison.
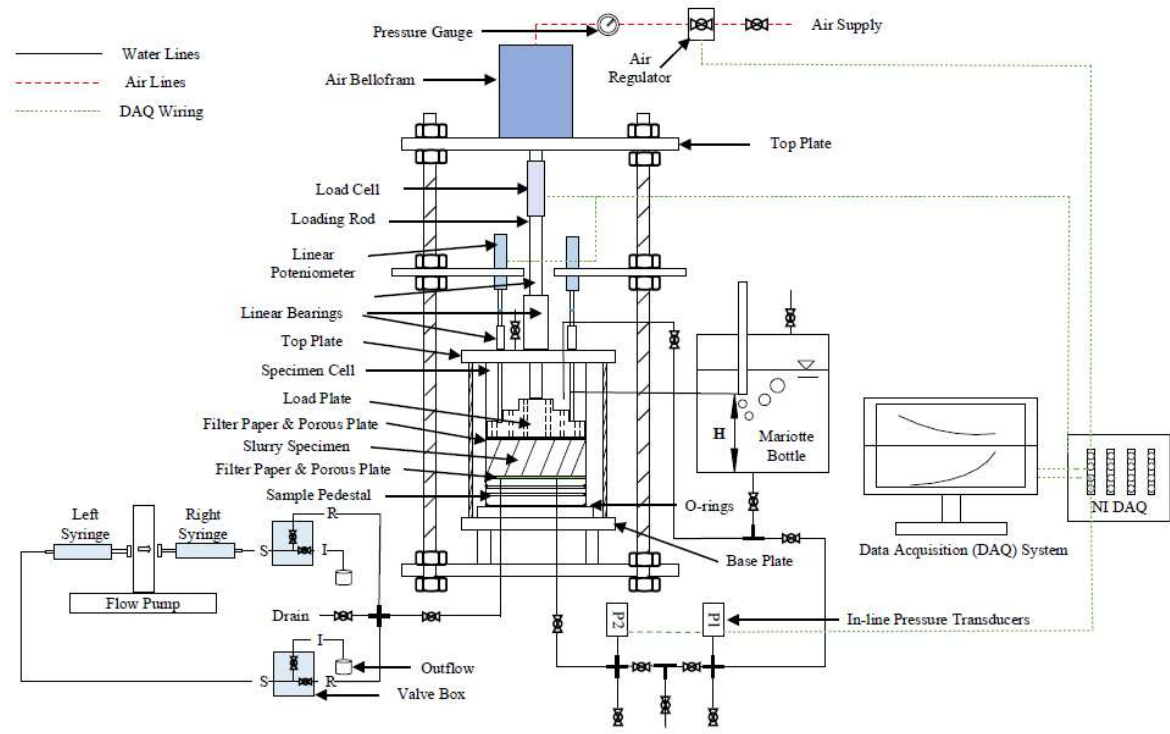
Fig. 3.3. Schematic of the seepage-induced consolidation test (SICT) apparatus (after Tian, 2017).
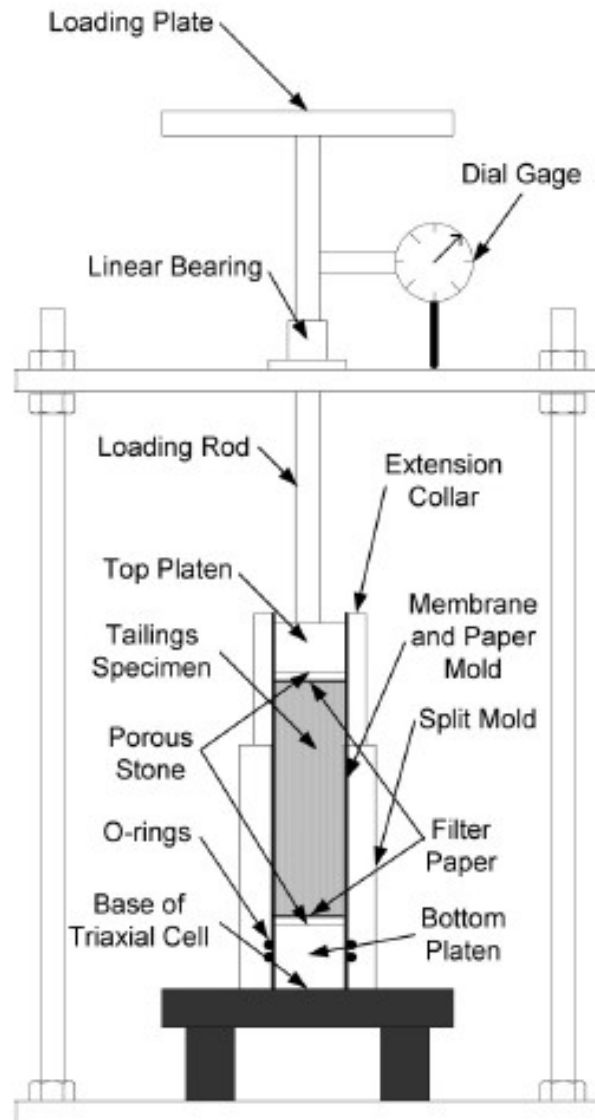
Fig. 3.4. Schematic of the consolidation frame used for preparation of specimens for triaxial compression testing (after Jehring & Bareither, 2016).
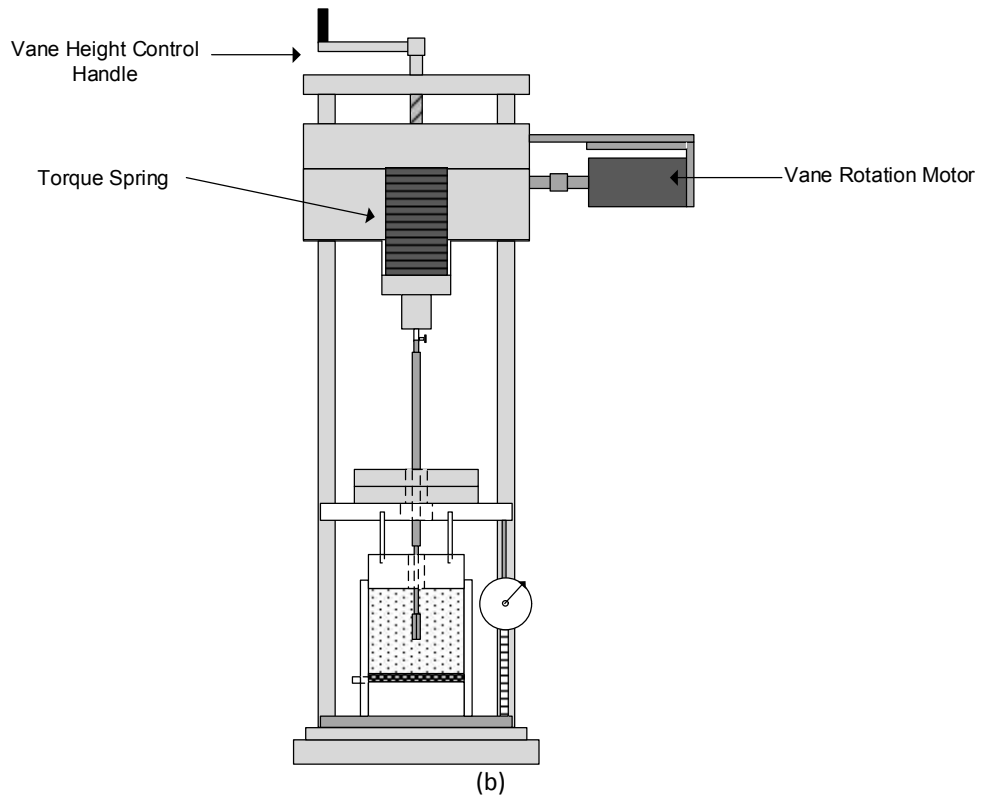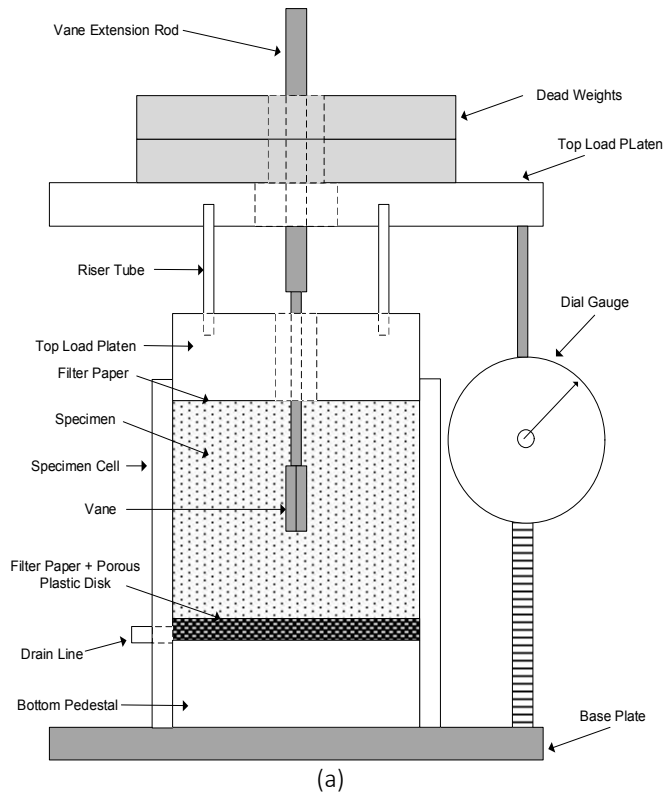
Fig. 3.5. Schematics of the small-scale vane shear consolidation cell and apparatus used for (a) consolidation, and (b) small-scale vane shear.
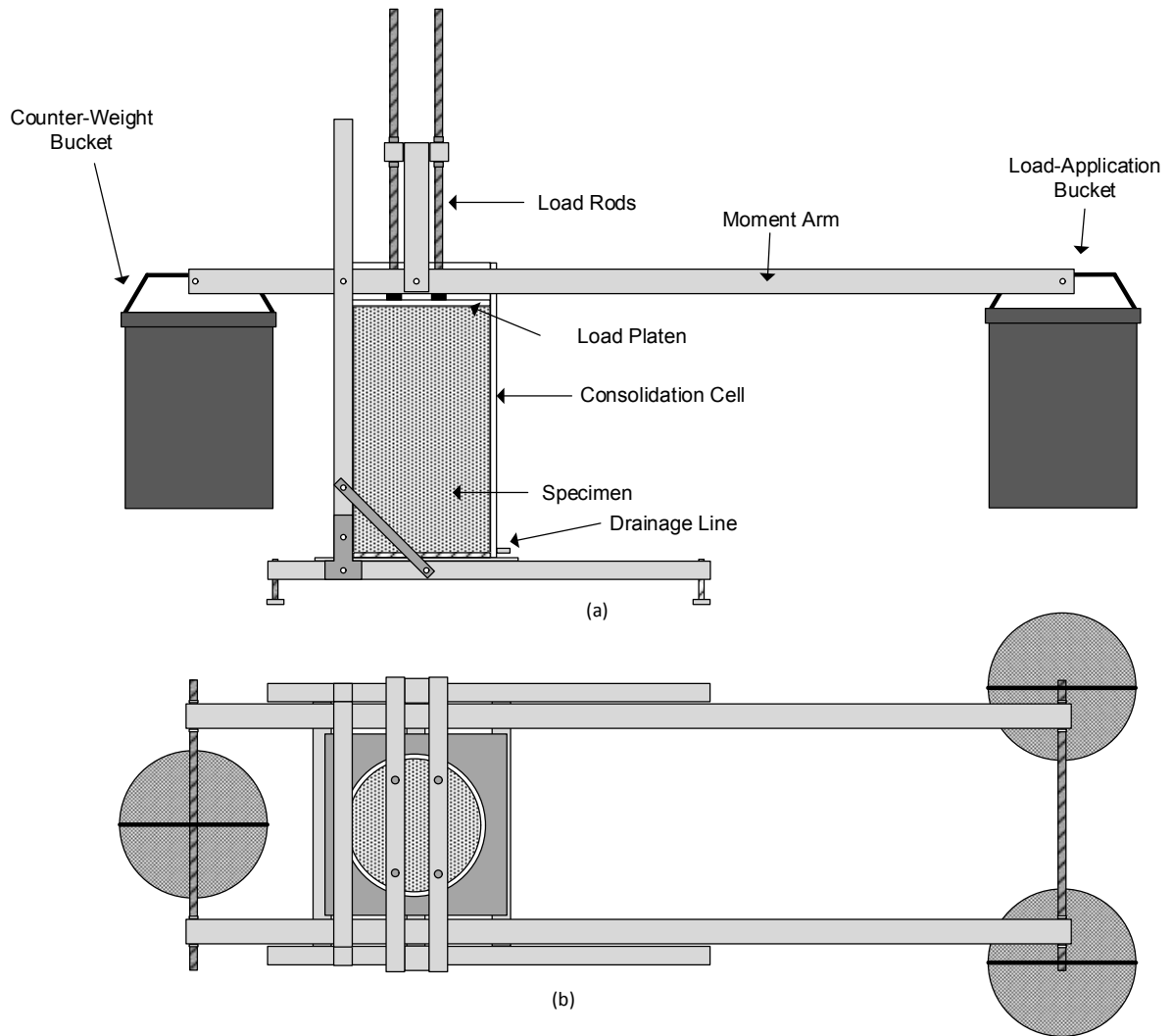
Fig. 3.6. Schematics of the large-scale vane shear consolidation cell and load frame in (a) cross-section, and (b) plan view.

CHAPTER 4: RESULTS AND DISCUSSION

Compressibility, hydraulic conductivity, and shear strength tests were conducted on CCP. Results from these experiments were used to assess how shear strength of CCP measured in vane shear compared with traditional laboratory methods. In particular, vane shear results were compared to drained and undrained strength envelopes developed through CU triaxial compression to assess drainage conditions of CCP during vane shear.

The discussion pertaining to CCP and vane shear was further supported by a series of vane shear tests on FST. Fine synthetic tailings was used since this material had a lower hydraulic conductivity compared to CCP (FST consisted of > 40% clay-sized particles). Thus, FST was well-suited for evaluation of S_u via vane shear as undrained conditions were maintained during shear.

4.1 Compressibility and Hydraulic Conductivity of CCP

Seepage-induced consolidation tests were conducted on CCP and the tests are summarized in Table 4.1 as SICT_1, SICT_2, and SICT_3. The summary in Table 4.1 includes the following: initial void ratio of the slurry specimens (e_i); void ratio at zero effective stress (e_0); initial height of the slurry specimen (H_i); initial height of the settled specimen prior to vertical loading (H_0); and height of solids (H_s). The three SICTs on CCP were conducted on similarly prepared test specimens to verify compressibility and hydraulic conductivity results, and also to assess repeatability. Importantly, SICT gave a measurement of the coefficient of consolidation (c_v) of CCP which indicated how quickly u_e dissipated. This was useful for anticipating the drainage conditions in CCP during vane shear.

33

4.1.1 Seepage-Induced Consolidation

Relationships of e-σ_v' from the three SICTs on CCP as well as a single composite compressibility model (Eq. 3.2) are shown in Fig. 4.1. The SICTs were performed to a final σ_v' = 80 kPa, which represented a reasonable upper-bound σ_v' likely to be encountered in CCP impoundments. The e-σ_v' data for all three SICTs displayed characteristic consolidation behavior, whereby e decreased with increasing σ_v'. Comparing e_i and e_0 in Table 4.1, a considerable reduction in e occurred as water was released from the CCP during sedimentation and self-weight consolidation. Subsequent loading during the seepage and vertical loading phases of the SICT led to smaller changes in void ratio. A decrease in void ratio from approximately 1.25 to 0.95 as σ_v' increased from 0.5 kPa to 80 kPa was evident in the e-σ_v' results (Fig. 4.1). The average compression index (C_c) of the CCP was 0.08. Although the compressibility of CCP was low given the relatively high initial void ratio, compressibility was typical of CCP (EPRI, 2012).

The e-k_s and k_s-σ_v' relationships for the three SICTs are shown in Fig. 4.2. Values of k_s decreased from 6 x 10^{-7} m/s to 2 x 10^{-7} m/s as σ_v' increased from 1.5 to 80 kPa. This magnitude of k_s was typical of CCP, as was the relative insensitivity of k_s to σ_v' (EPRI, 2012). In general, there was good agreement between compressibility and hydraulic conductivity behavior of the three SICTs on CCP. Minor differences were attributed to measurements of the initial specimen height via the adhered measuring tape on the outside of the SICT cell and minor loss of material via squeezing out along the side of the load platen. Measurements of the initial specimen height via the ruler adhered to the side of the specimen cell had an accuracy of ±0.5 mm.

4.1.2 Time-Rate of Consolidation

Time-rate of consolidation observed in SICT_2 on CCP is shown in Fig. 4.3a. The u_e and vertical deformation (δ_v) are plotted for the load increment from σ_v' = 20 kPa to σ_v' = 40 kPa that was induced by the vertical load piston. The average specimen height was 43 mm and drainage

was only allowed via the top boundary such that u_e was monitored at the bottom boundary. At time (t) = 0, u_e = -1 kPa because the vertical load was applied directly after using the flow pump to provide suction to measure hydraulic conductivity under the previous load increment. Developed u_e due to loading completely dissipated after approximately 2.5 min (150 s). Only 22% of the applied vertical load was measured as u_e due to the high k_s and rapid drainage of CCP. The square-root of time method was used to determine the coefficient of consolidation (c_v), and c_v = 1.25 m^2/d was computed based on data shown in Fig. 4.3a. The c_v for CCP was relatively consistent across the entire range of σ_v' used to evaluate compressibility.

Deformation versus square root of time relationships for load increments during consolidation of CCP specimens in direct shear, SS-VS, and LS-VS are shown in Fig. 4.3b. The c_v for the direct shear and vane shear specimens were determined using the square-root of time method. For a stress increment from σ_v' = 20 kPa to σ_v' = 40 kPa, the SS-VS and LS-VS specimens yielded c_v = 1.19 m^2/d and 0.89 m^2/d, respectively. The direct shear specimen yielded c_v = 1.20 m^2/d for a stress increment from σ_v' = 10 kPa to σ_v' = 20 kPa. These c_v were comparable to the c_v calculated using the SICT, which indicates that time-rate of consolidation behavior was consistent across all laboratory experiments conducted on CCP.

The c_v of CCP was relatively high compared to most natural fine-grained materials. A high c_v indicates rapid dissipation of u_e and rapid settlement. A c_v = 1.25 m^2/day, based on SICT data, was used to approximate the time required for 99% consolidation for a given load increment of a given CCP test specimen (e.g., LS-VS specimen with height = 600 mm and double-drainage yielded t_{99} = 3.08 hr). The analysis of time-rate of consolidation of CCP ensured that suitable elapsed times between load increments in any laboratory experiment on CCP were allowed to complete consolidation. Furthermore, the high c_v meant that undrained conditions were unlikely to be maintained during vane shear and instead partially drained conditions would develop.

4.1.3 Test Specimen Consolidation

A compilation of e versus σ_v' is shown in Fig. 4.4 for all SICT, triaxial, direct shear, SS-VS, and LS-VS specimens evaluated in this study. All void ratios in Fig. 4.4 for shear strength experiments are final void ratios prior to shearing. In general, consistent void ratios under a given σ_v' were achieved among the different experiments. Scatter in the SS-VS data was due to slight inaccuracy in measuring the final specimen thickness and w. Ponded water on the surface of the SS-VS specimens at the end of testing meant that the final w was likely overestimated. For example, variation in the final water content of $\pm 2\%$ led to e ± 0.05 for the final void ratio. This variation in the final void ratio is comparable to the range of scatter observed in Fig. 4.4.

Data from the triaxial test specimens in Fig. 4.4 were plotted relative to σ_v' at the end of consolidation, which was equal to σ_c'. Modestly lower void ratios for triaxial specimens were observed for a given σ_v' because triaxial specimens were isotropically consolidated, compared to all other specimens that were anisotropically consolidated. The larger component of lateral effective stress in triaxial specimens due to isotropic consolidation increased compression and decreased void ratio.

4.2 Shear Strength of CCP

Shear strength of CCP was evaluated via three different laboratory techniques: direct shear, triaxial compression, and vane shear. Furthermore, vane shear was conducted in SS-VS and LS-VS. Triaxial compression tests were used to determine drained and undrained shear strength of CCP. Direct shear tests were conducted to determine a second measure of drained shear strength on CCP and compare with drained strength measured in triaxial compression. These measurements of CCP shear strength were used to create baseline conditions of drained and undrained shear strength to assess measurements of shear strength from vane shear.

4.2.1 Consolidated Undrained Triaxial

Consolidated undrained triaxial compression tests are summarized in Table 4.2. The data compilation in Table 4.2 includes the following: σ_c', axial strain at failure ($\varepsilon_{a,f}$), deviator stress at failure ($\Delta\sigma_{d,f}$), effective major principle stress at failure (σ_{1f}'), effective minor principle stress at failure (σ_{3f}'), p' and q at failure, excess pore water pressure at failure ($u_{e,f}$), secant friction angle (ϕ_{sc}'), B-value, and e_f.

4.2.1.1 Shear Behavior

Relationships of $\Delta\sigma_d$ and u_e versus ε_a for CU triaxial tests are shown in Fig. 4.5a. Triaxial tests on CCP were performed at σ_c' = 10, 20, 50, and 100 kPa and sheared to ε_a = 20%. The CCP exhibited a tendency to contract on initial loading followed by a tendency to dilate with continued axial deformation. Contractive behavior and development of positive u_e was more pronounced at higher σ_c', which was attributed to suppressed dilatancy with increasing σ_c'. However, all specimens did exhibit a modest tendency to dilate with increased axial deformation that led to strain-hardening behavior, whereby $\Delta\sigma_d$ increased before becoming approximately constant near the end of the experiment (i.e., $\varepsilon_a \approx 20\%$). The undrained shear behavior of CCP agrees with that of loosely-prepared, low-plasticity silts (Brandon, et al. 2006, Wang & Luna 2012).

4.2.1.2 Evaluation and Definition of Failure

A definition of failure during laboratory CU triaxial testing is needed to determine shear strength parameters that can best represent a given engineering scenario. The six failure criteria described by Brandon et al. (2006) were considered. In this study, the point at which an effective stress path for a given CU triaxial test specimen reached the K_f line was used to define failure. Selection of this failure criterion was based on previous work conducted by Jehring and Bareither (2016).

Effective stress paths in *p'-q* space reach the K_f line at failure and theoretically maintain a constant *q/p'* ratio for the remainder of axial deformation in a CU triaxial test. In this study, all CCP specimens were normally consolidated materials such that the K_f line was assumed to pass through the origin (i.e., *p'* = 0 and *q* = 0). Thus, for a set of *p'-q* data from an individual CU test specimen, all data points that yielded approximately the same *q/p'* ratio were included in a linear regression to determine a K_f line for that specimen. The first *p'-q* point to plot on the K_f line for a given test was taken as the stress state at failure. A composite K_f line was computed for all CU tests at multiple σ_c'. This was done by plotting all *p'-q* data points where a constant *q/p'* ratio had been reached. The slope of the composite K_f line was then used to compute the effective friction angle (ϕ').

4.2.1.3 Shear Strength

Effective stress paths in *p'-q* space for the four CU triaxial compression tests on CCP are shown in Fig. 4.6. The K_f line shown in Fig. 4.6, was regressed through all *p'-q* points that defined a common K_f line. The initial *p'-q* point that fell on the K_f line was characterized qualitatively as the start of a relatively constant *q/p'* ratio, and all subsequent *p'-q* points were assumed to represent failure conditions. The slope of the K_f line (α) for CCP was 0.59, which yielded ϕ' = 36°.

Drained and undrained Mohr-Coulomb strength envelopes for CCP are shown in Fig. 4.7. Effective stress and total stress Mohr circles were drawn to represent the stress states at failure. The drained strength envelope was previously evaluated based on the K_f line and had a slope of ϕ' = 36°. The drained strength envelope was tangent to the effective stress Mohr circles. The undrained strength envelope was determined by fitting an envelope tangent to the total stress Mohr circles. The slope of the undrained strength envelope for CCP corresponded to a total stress friction angle (ϕ) of 20°. Good agreement between drained and undrained strength envelopes

from each triaxial test indicated that the shear strength of CCP was effectively captured by the CU triaxial compression tests.

4.2.2 Consolidated Drained Direct Shear

A summary of the consolidated drained direct shear tests conducted on CCP is in Table 4.3. The data compilation in Table 4.3 includes σ_v', τ_p, initial void ratio prior to shear (e_i), and e_f. Multiple direct shear tests were conducted at σ_v' = 32, 48, and 110 kPa to account for potential minor inconsistencies between specimens and to assess repeatability.

Relationships of τ and e versus horizontal displacement (δ_h) for the direct shear tests on CCP are shown in Fig. 4.8. In all direct shear tests the CCP exhibited contractive behavior. The contractive behavior corresponded to a strain-hardening response under drained conditions, whereby the material became denser with increasing δ_h and τ increased and ultimately reached a constant magnitude. This shear behavior is typical for loose, low plasticity silts. The τ_p for a given test was defined as the maximum τ measured during the test. In all direct shear tests, τ_p increased with increasing σ_v' due to increased density (i.e., lower void ratio, Fig. 4.8b) that generated greater frictional resistance between particles.

Relationships between the ratio of shear stress to vertical effective stress (τ/σ_v') versus δ_h for direct shear tests on CCP are shown in Fig. 4.9. Nearly all direct shear tests achieved a similar ratio of τ/σ_v', which indicated similar secant friction angles and a linear strength envelope for CCP could be developed that passed through the origin. Test DS_3 at σ_v' = 32 kPa was a single outlier in the direct shear data set and achieved a higher τ/σ_v' ratio than all other tests. Although this test was included in the analysis, the dissimilarity in shear behavior relative to all other direct shear tests suggests that DS_3 was not an effective representation of the drained shear strength of CCP. The reason for this different behavior is unknown.

The drained and undrained strength envelopes for CCP established from CU triaxial tests are reproduced in Fig. 4.10 along with τ_p versus σ_v' points representing failure conditions in the direct shear tests. The failure conditions established from the drained direct shear tests compare favorably to the drained strength envelope determined from the CU triaxial tests, which further supports the definition of failure and ϕ' established in the CU triaxial tests. Modest deviation of the τ_p-σ_v' failure points in direct shear were observed at the highest level of σ_v', which may be attributed to different stress conditions during consolidation and at failure between the direct shear and triaxial compression. For example, triaxial specimens were isotropically consolidated leading to denser specimens prior to shear (Fig. 4.4), which can correspond to higher shear strength.

4.2.3 Vane Shear Tests

A summary of all SS-VS tests and LS-VS tests conducted on CCP is in Table 4.4. The data compilation in Table 4.4 includes the following: σ_v', τ_p, residual shear strength (τ_r), rate of vane rotation, time delay between vane insertion and beginning rotation (t_d), elapsed time under the final σ_v' (t_c), and e_f.

4.2.3.1 Effect of Rate of Rotation

The relationship between τ_p versus rate of vane rotation for SS-VS tests conducted on CCP specimens consolidated to σ_v' = 95 kPa is shown in Fig. 4.11. The rate of vane rotation influences the time to failure, which controls the available time for drainage of u_e developed during shear. The standard rate of rotation for a miniature vane is between 30 °/min and 60 °/min. Shear rates corresponding to 5 °/min, 60 °/min, 150 °/min and 240 °/min were considered for the CCP. The measured τ_p was approximately constant with respect to rate of rotation in SS-VS (Fig. 4.11). The absence of any influence of rate of rotation on τ_p was attributed to the high c_v for CCP and small vane diameter, which likely promoted drained conditions during shear.

Blight (1959) discussed the effect of rate of vane rotation in silty materials. Blight developed a relationship between degree of drainage during vane rotation and a dimensionless time factor (Fig. 2.2). The time factor was a function of c_v, time to failure (measured from the start of rotation), and vane diameter. Blight assumed undrained conditions when the degree of drainage was less than 10%. All time factors for SS-VS tests in which the rate of rotation was varied were compared to the relationship proposed by Blight in Fig. 4.12. Even with a rate of rotation of 240 °/min, a degree of drainage significantly more than 10% was achieved, which suggests partially-drained to fully-drained conditions developed. Based on Fig. 4.12, to test CCP under undrained conditions with a 12.7-mm-diameter vane failure would have to be reached almost instantaneously, which can be considered impractical for vane shear testing.

4.2.3.2 Effect of Delay Prior to Shear

The relationship of τ_p versus time delay between vane insertion and beginning rotation (t_d) for SS-VS tests conducted on CCP specimens consolidated to $\sigma_v' = 95$ kPa is shown in Fig. 4.13. The standard t_d was one minute, and t_d was varied between 0 and 60 min. Similar to rate of rotation, there was no defined trend between τ_p and t_d across the range of elapsed times evaluated. Furthermore, the collection of SS-VS tests presented in Fig. 4.11 and Fig. 4.13 indicate that τ_p for CCP consolidated to $\sigma_v' = 95$ kPa and maintained under that load for 24 hr ranged between approximately 16 and 22 kPa, with an average $\tau_p = 18.4 \pm 1.7$ kPa.

Morris and Williams (2000) reported that vane insertion can lead to development of u_e up to 75% of σ_v' during a given vane shear test. Subsequent dissipation of u_e after vane insertion produces an increase in effective stress and a corresponding increase in vane shear strength. Vane shear tests on materials with c_v lower than CCP and with larger vane diameters than what was used in the SS-VS tests in this study showed an increase of measured shear strength up to 126% with increasing t_d (Morris & Williams, 2000). The high c_v of CCP combined with the relatively

small vane diameter used in the SS-VS tests meant that even after the shortest delays (i.e., shearing immediately after vane insertion), u_e due to vane insertion had dissipated. The similarities in τ_p measured in SS-VS on CCP with varying rate of rotation and elapsed time following vane insertion suggest that CCP was readily drained and τ_p can be assumed to represent drained shear strength.

4.2.3.3 Effect of Diagenesis

Relationships of τ_p and τ_r versus elapsed time under a constant σ_v' (t_c) for SS-VS tests conducted on CCP specimens consolidated to σ_v' = 95 kPa are shown in Fig. 4.14. Both τ_p and τ_r were observed to increase with increasing t_c up to an approximately constant strength after 72 hr in the consolidation cell under a constant σ_v'. These trends indicate that the shear strength of CCP is controlled by physical processes and also the time-dependent chemical diagenesis. EPRI (2012) showed that diagenesis increased the stiffness of CCP, and increased stiffness can be correlated to increased peak shear strength.

The magnitudes of τ_p and τ_r in Fig. 4.14 indicate that CCP is a sensitive material, whereby a considerable loss in strength is observed between τ_p and τ_r. The ratio of τ_p/τ_r increased with increasing time to t_c = 72 hr and ranged between 8 and 16 for all t_c > 1 hr. The strength loss due to disturbance and remolding suggests that shearing eliminated any strength gain due to diagenesis in the CCP, leading to very low τ_r, irrespective of t_c.

Diagenesis that was evaluated in SS-VS testing was accounted for in the CU triaxial and direct shear tests. All CU triaxial tests were conducted after at least 48 hr had elapsed under the final σ_c'. In addition, direct shear tests were conducted at least 24 hr after applying the final σ_v'. Based on the vane shear results presented in Fig. 4.13, complete diagenesis in the CCP may not have occurred in the direct shear test specimens. The shorter elapsed time under σ_v' for the direct shear test specimens further accounts for the modest difference (lower strengths) observed

between shear strength measured via direct shear and the drained strength envelope developed from CU triaxial testing.

4.2.3.4 Shear Strength

The evaluations of rate of vane rotation, elapsed time between vane insertion and shearing, and elapsed time under constant σ_v' prior to shear in SS-VS yielded two important observations: (i) CCP exhibited drained shear, even at fast rates of rotation; and (ii) diagenesis increases τ_p such that elapsed time under constant σ_v' prior to shear needs to be accounted for in vane shear testing of CCP. Measurements of τ_p in LS-VS were conducted at σ_v' = 40 and 88 kPa and accounted for slow rates of rotation and a t_c = 120 hr. The measured τ_p in LS-VS_1 and LS-VS_3 were comparable to SS-VS tests conducted under similar conditions (Table 4.4). For example, the LS-VS_1 test conducted under σ_v' = 88 kPa yielded τ_p = 25 kPa, which was comparable to the maximum τ_p measured in SS-VS that accounted for development of diagenesis at elapsed times under constant σ_v' of 72 and 168 hr (SS-VS_16 and 17, Table 4.4). Thus, for the vane shear experiments conducted in this study, comparable measurements of τ_p were obtained in SS-VS and LS-VS under similar experimental conditions.

The tests labeled as LS-VS_2 and LS-VS_4 were conducted on CCP that had previously been tested (i.e., for LS-VS_1 and LS-VS_3) and subsequently air-dried before being reused to prepare a new slurry specimen. Both these repeat tests exhibited lower shear strength than the previous tests under similar conditions (LS-VS_1 and LS-VS_3). This reduction in shear strength was attributed to a reduction in the effect of diagenesis on the CCP caused by remolding and destruction of the initial bonds formed via diagenesis and a subsequent wet-dry cycle. Although only two LS-VS shear tests were conducted that unknowingly evaluated this phenomenon, the ≈ 20% reduction in τ_p measured for both CCP specimens subjected to remolding and a second wet-dry support the hypothesis.

Relationships of τ_p versus the total horizontal and vertical stress (σ_h and σ_v) in the SS-VS and LS-VS tests are shown in Fig. 4.15 along with the drained and undrained strength envelopes determined from the CU triaxial tests on CCP. The vane shear data in Fig. 4.15 indicate that τ_p plotted with respect to σ_h provides a more appropriate fit to the strength envelopes developed from the CU triaxial tests. The σ_h was computed based on the σ_v' prior to shear and assuming (i) at-rest (K_0) conditions with $\phi' = 36^\circ$ and $K_0 = 1 - \sin(\phi')$ and (ii) initial pore water pressure prior to shear was zero. Thus, assuming $u_e \approx 0$ during vane shear testing on CCP, the horizontal effective stress (σ_h') would be equal to σ_h'; σ_h' was used herein since the actual drainage conditions during vane shear were unknown and inferred from comparisons to drained and undrained strength envelopes.

The assumption that σ_h' more appropriately represented the effective stress acting on the failure surface prior to shearing was validated by considering the failure surface developed during vane shear failure. Conventional vane shear strength interpretation is derived based on a cylindrical failure surface, with shear resistance provided by the vertical sides of the cylinder and the horizontal ends (Fig. 2.1). Assuming a vane H/D ratio = 2 and conventional stress distribution around the cylindrical surface, the vertical shear surface contributes 86% of shear resistance (Chandler, 1988). Furthermore, Kouretzis et al. (2017) indicated that vane shear strength is analogous to direct simple shear conditions in the vertical plane, under a normal effective stress equal to $\sigma_h' = K_0 \cdot \sigma_v'$. Therefore, τ_p was best represented versus σ_h' on the Mohr-Coulomb envelope for vane shear tests.

The LS-VS and SS-VS failure points plotted as τ_p versus σ_h in Fig. 4.15 generally fall between the drained and undrained strength envelopes established in CU triaxial compression. Points plotting below the undrained strength envelope were for tests in which t_c was short and limited the effect of diagenesis. Four tests are identified in Fig. 4.15 where tests conditions were such that complete diagenesis occurred. In general, shear strength measured from these tests

plotted on or closer to the drained strength envelope relative to all other vane shear tests. This overestimation of undrained shear strength of CCP in vane shear can be explained by the drainage conditions that developed during the test. Vane shear tests were developed to measure undrained shear strength of soft, high plasticity clays. Standard procedures were developed to ensure undrained conditions were maintained during the entire testing process. Low plasticity silts, such as CCP, have considerably higher permeability than high plasticity clays, and can lead to partially-drained or even fully-drained conditions during vane shear. The development of partially-drained or fully-drained conditions in CCP was supported by the fact that nearly all shear strength results from vane shear plot between the undrained and drained strength envelopes.

4.3 Shear Strength of FST

Small-scale vane shear tests conducted on FST are summarized in Table 4.5. These tests were conducted to assess the specimen preparation and methodology for the SS-VS test, as well as provide further evidence to explain drainage conditions developed during vane shear testing. As previously noted, FST had higher plasticity and lower hydraulic conductivity compared to CCP, which made FST better suited to vane shear testing as undrained conditions more than likely would be established during shear following the ASTM standard procedure.

4.3.1 Shear Strength

Drained and undrained strength envelopes for FST are shown in Fig. 4.16 that were adopted from CU triaxial tests conducted by Hamade (2017), whereby $\phi' = 39°$ and $\phi = 15°$. Also included in Fig. 4.16 are relationships of τ_p versus the total vertical and horizontal stress (σ_v and σ_h) in the SS-VS tests conducted on FST. Similar to the CCP analysis, σ_h more effectively represented the stress state at failure during the vane shear test for FST. A total of five SS-VS tests were conducted across a range of σ_v', with a portion of tests repeated. There was good

45

agreement between the repeated vane shear tests and data plotted along a consistent strength envelope. The strength envelope from the SS-VS tests showed good agreement with the undrained strength envelope for FST, with the exception of SS-VS_24 that appeared to be an outlier. Effective measurement of S_u and agreement with the undrained strength envelope was anticipated since k_s for FST was approximately 7.24 x 10^{-9} m/s and c_v = 0.010 m^2/day (Tian, 2017), which supported undrained conditions during vane shear.

Drainage conditions during vane shear were assessed based on the method described by Blight (1968). Blight recommends a degree of consolidation of less than 10% in order to ensure undrained conditions are being measured. Fig. 4.12 illustrates that a degree of drainage less than 10% was maintained during all SS-VS tests on FST, except one test, which significantly overestimated the undrained shear strength (SS-VS_24). These results demonstrate that the SS-VS test provided a reasonable estimate of S_u for FST, largely due to the low permeability.

4.4 Practical Implications

Understanding the shear strength of deposited CCP is important for safe construction and to avoid catastrophic failure. The data herein support that vane shear tests may overestimate the undrained strength of CCP and show closer approximation to the drained strength envelope. If undrained conditions do develop during loading of CCP, particularly during construction, the shear strength measured from the vane shear may not be representative of the conditions in the field and could lead to an unconservative design.

Diagenesis is shown to significantly improve the strength of CCP. However, data herein shows that disturbance of the CCP eliminates any of the strength gain due to diagenesis, leading to residual shear strength that is much lower than the peak shear strength. Therefore, reliance on the peak strength may also be unconservative. Disturbance due to construction equipment may eliminate any strength gain due to diagenesis. Observations in the laboratory showed that

material consolidated to relatively high stresses (i.e. $\sigma_v' = 100$ kPa) had reasonably high measured shear strength when undisturbed, however, inducing vibration lead to the material losing almost all strength and being able to flow. This is likely due to the elimination of any strength gain due to diagenesis, as well as the high retained water content even under high vertical stresses.

The preparation of remolded laboratory samples of CCP requires that diagenesis be accounted for. The results herein show that CCP gains strength with time and that testing materials after 12 hours of 72 hours yields very different results. A consistent sample preparation procedure is needed when testing CCP to ensure that the effects of diagenesis are controlled and that the sample is representative of the in situ conditions.

Table 4.1. Summary of the three seepage-induced consolidation tests (SICTs) conducted on coal combustion product (CCP).

Test	e_i	e_0	H_i (mm)	H_0 (mm)	H_s (mm)
SICT_1	3.53	1.50	67	37	15
SICT_2	3.18	1.41	92	53	22
SICT_3	2.00	1.27	99	75	33

Notes: e_i = initial void ratio of slurry; e_0 = void ratio at zero effective stress; H_i = initial height of slurry sample; H_0 = height at zero effective stress; H_s = initial height of solids in sample.

Table 4.2. Summary of consolidated-undrained triaxial compression tests conducted on coal combustion product (CCP).

Test	σ_c' (kPa)	$\varepsilon_{a,f}$	$\Delta\sigma_{d,f}$ (kPa)	σ_{3f}' (kPa)	σ_{1f}' (kPa)	p' (kPa)	q (kPa)	$u_{e,f}$ (kPa)	ϕ_{sc}'	B-value	e
CU_1	9.7	2.5%	22.2	7.6	29.8	18.7	11.1	2.1	36.4	0.97	0.98
CU_2	20.0	2.2%	36.7	14.9	51.6	33.2	18.4	5.1	33.5	0.96	0.96
CU_3	50.3	2.2%	55.5	25.0	80.5	52.7	27.8	25.0	31.8	0.95	0.92
CU_4	100	3.1%	108.7	41.9	150.6	96.3	54.4	58.1	34.4°	0.96	0.90

Notes: σ_c' = effective confining stress; $\varepsilon_{a,f}$ = axial strain at failure; $\Delta\sigma_{d,f}$ = deviator stress at failure; σ_{3f}' = minor effective principal stress at failure; σ_{1f}' = major effective principal stress at failure; p' = mean effective stress at failure; q = mean shear stress at failure; $u_{e,f}$ = excess pore water pressure at failure; ϕ_{sc}' = secant friction angle; B-value = b-check for saturation; e = global void ratio before shear.

Table 4.3. Summary of consolidated-drained direct shear tests conducted on coal combustion product (CCP).

Test	σ_v' (kPa)	τ_p (kPa)	e_i	e_f
DS_1	32.7	22.7	1.05	0.90
DS_2	32.7	20.3	1.05	0.96
DS_3	32.7	28.7	1.06	0.93
DS_4	48.2	29.3	1.03	0.94
DS_5	48.2	26.7	1.02	0.97
DS_6	48.2	30.7	1.03	0.95
DS_7	48.2	30.0	1.02	0.96
DS_8	110.1	69.1	1.00	0.93
DS_9	110.1	69.0	0.99	0.97
DS_10	110.1	62.0	1.00	0.93
DS_11	110.1	65.9	1.00	0.90
DS_12	110.1	69.2	1.01	0.99

Notes: σ_v' = vertical effective stress; τ_p = peak shear stress; e_i = void ratio before shear; e_f = void ratio after shear.

Table 4.4. Summary of small-scale vane shear (SS-VS) and large-scale vane shear (LS-VS) tests conducted on coal combustion product (CCP).

Test Type	σ_v' (kPa)	σ_h' (kPa)	τ_p (kPa)	τ_r (kPa)	Rate of Rotation (°/min)	t_d (min)	t_c (hr)	e
SS-VS_1	38.6	15.9	1.67	0.36	60	1.0	24	1.01
SS-VS_2	38.6	15.9	4.93	1.02	60	1.0	24	1.02
SS-VS_3	63.3	26.1	14.23	1.67	60	1.0	24	0.98
SS-VS_4	63.3	26.1	13.09	1.42	60	1.0	24	0.99
SS-VS_5	94.3	38.9	19.29	1.59	60	1.0	24	1.00
SS-VS_6	94.3	38.9	16.84	1.18	60	0.0	24	1.01
SS-VS_7	94.3	38.9	21.41	2.48	60	20.0	24	0.97
SS-VS_8	94.3	38.9	17.50	1.18	60	60.0	24	1.00
SS-VS_9	94.3	38.9	18.31	0.85	5	1.0	24	0.98
SS-VS_10	94.3	38.9	15.54	1.18	150	1.0	24	0.97
SS-VS_11	94.3	38.9	2.16	0.85	60	1.0	1	0.98
SS-VS_12	94.3	38.9	3.30	0.36	60	1.0	6	1.02
SS-VS_13	94.3	38.9	10.97	1.34	60	1.0	12	0.99
SS-VS_14	94.3	38.9	19.29	1.67	200	1.0	24	1.00
SS-VS_15	94.3	38.9	19.29	2.16	280	0.0	24	1.01
SS-VS_16	94.3	38.9	26.14	1.67	60	1.0	72	0.97
SS-VS_17	94.3	38.9	24.35	2.32	60	1.0	168	0.99
LS-VS_1	87.9	36.2	25.00	3.00	12	5.0	120	0.95
LS-VS_2	87.9	36.2	21.00	2.00	12	5.0	120	0.95
LS-VS_3	40.0	16.5	9.75	1.50	12	5.0	120	0.96
LS-VS_4	40.0	16.5	7.5	1.00	12	5.0	120	0.95

Notes: σ_v' = vertical effective stress prior to shear; σ_h' = horizontal effective stress prior to shear; τ_p = peak shear stress; τ_r = residual shear stress; t_d = time delay between vane insertion and beginning rotation; t_c = time in cell; e = global void ratio prior to shear.

Table 4.5. Summary of small-scale vane shear (SS-VS) conducted on fine synthetic tailings (FST).

Test Type	σ_v' (kPa)	σ_h' (kPa)	τ_p (kPa)	τ_r (kPa)	Rate of Rotation (°/min)	t_d (min)	t_c (hr)	e
SS-VS_18	16.9	6.3	1.67	1.18	60	1.0	120	1.43
SS-VS_19	32.4	12.0	3.30	0.77	60	1.0	120	1.26
SS-VS_20	32.4	12.0	3.14	2.16	60	1.0	120	1.22
SS-VS_21	63.3	23.5	7.71	2.65	60	1.0	120	1.08
SS-VS_22	63.3	23.5	6.56	2.16	60	1.0	120	1.10
SS-VS_23	63.3	23.5	8.68	3.46	60	1.0	120	1.06
SS-VS_24	94.3	38.9	18.64	7.87	60	1.0	120	0.99
SS-VS_25	94.3	38.9	9.34	-	60	1.0	120	1.00
SS-VS_26	94.3	38.9	10.96	4.44	60	1.0	120	1.08

Notes: σ_v' = vertical effective stress prior to shear; σ_h' = horizontal effective stress prior to shear; τ_p = peak shear stress; τ_r = residual shear stress; t_d = time delay between vane insertion and beginning rotation; t_c = time in cell; e = global void ratio prior to shear.
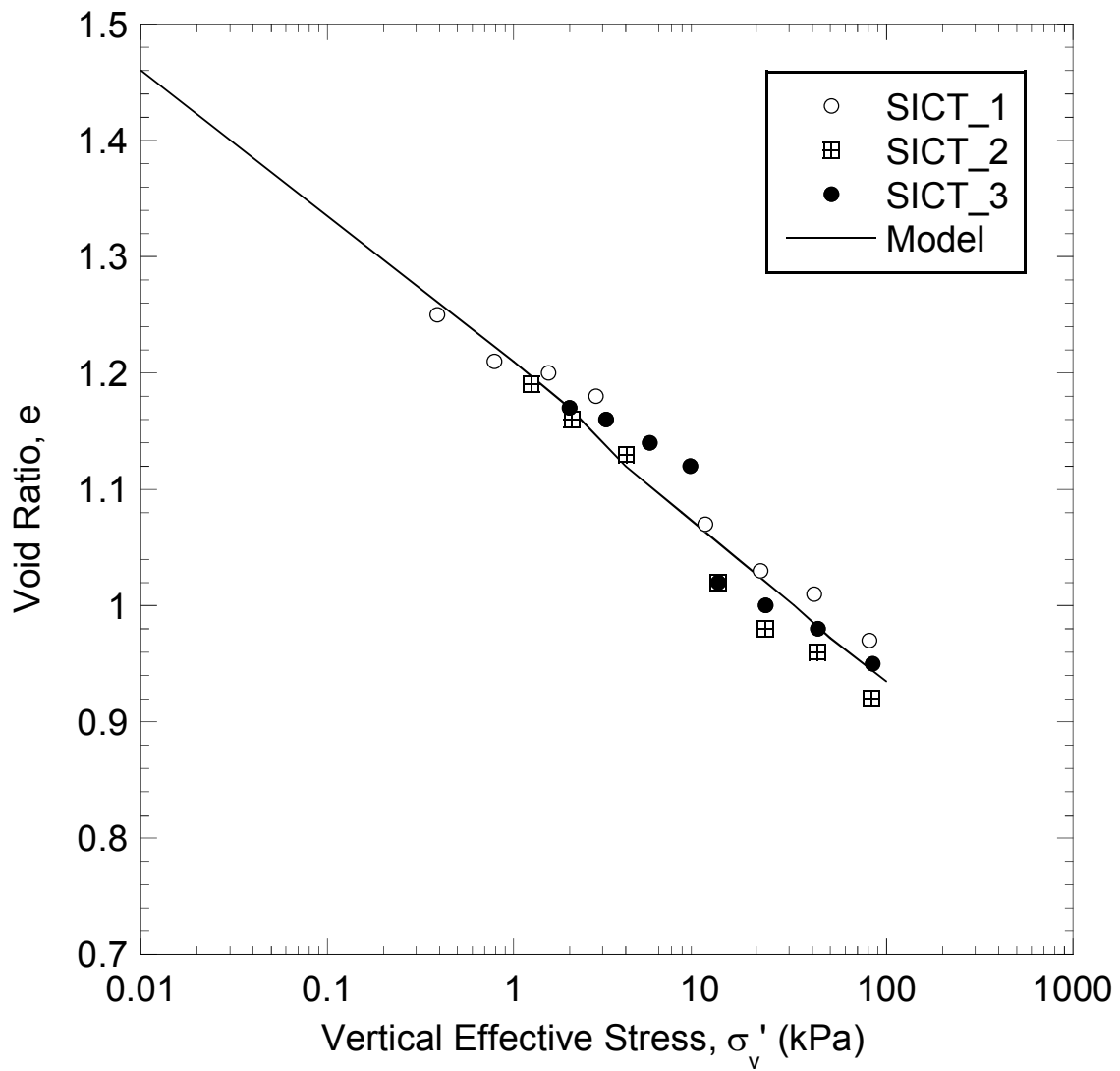
Fig. 4.1. Relationship of void ratio versus vertical effective stress for seepage induced consolidation tests (SICT) on CCP. Data points are representative of the mid-depth of a specimen at the end of consolidation during the seepage and loading phases. The SICT model was fit through the compilation of all test data.
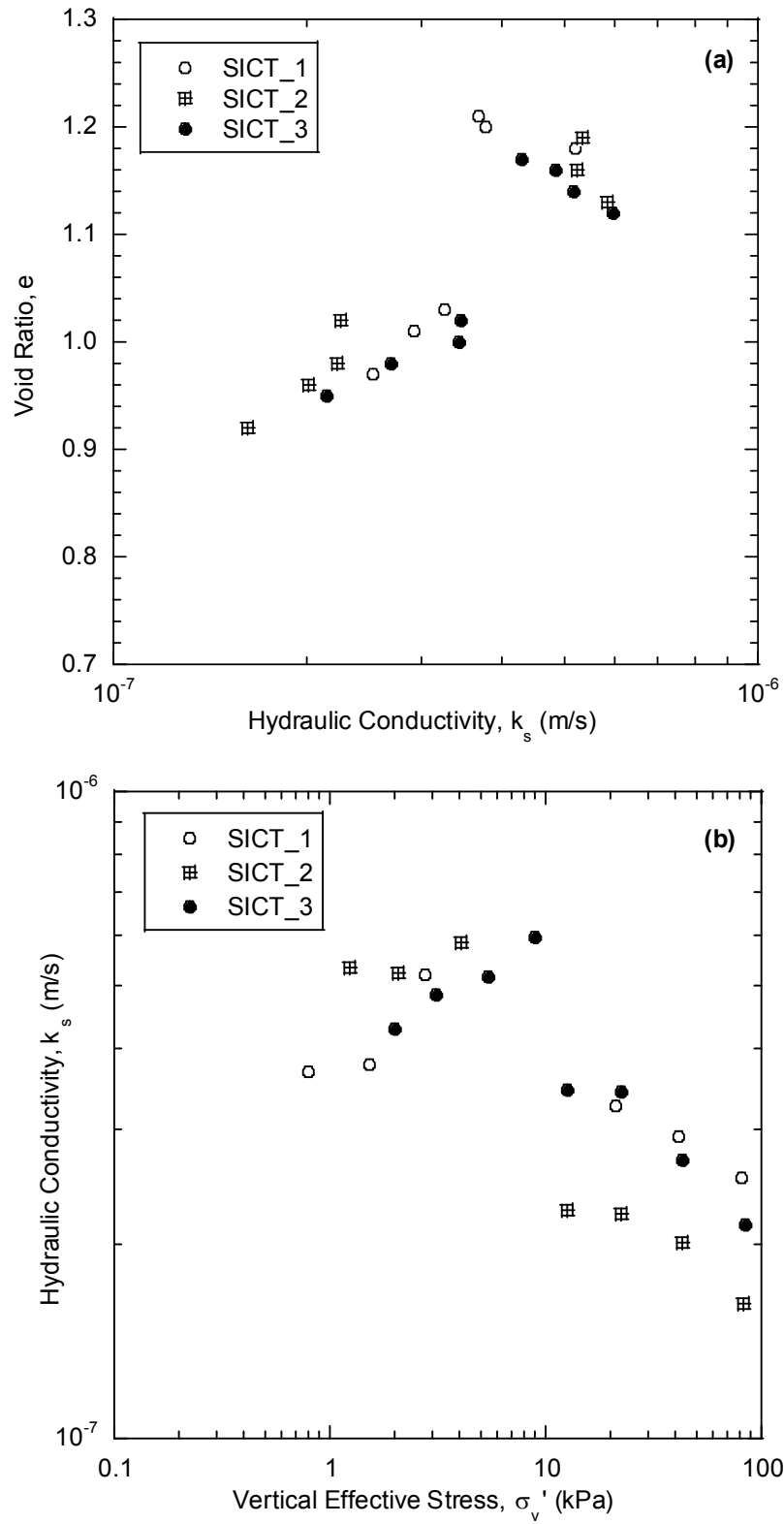
Fig. 4.2. Relationships of (a) void ratio versus saturated hydraulic conductivity and (b) saturated hydraulic conductivity versus vertical effective stress for seepage induced consolidation tests on CCP.
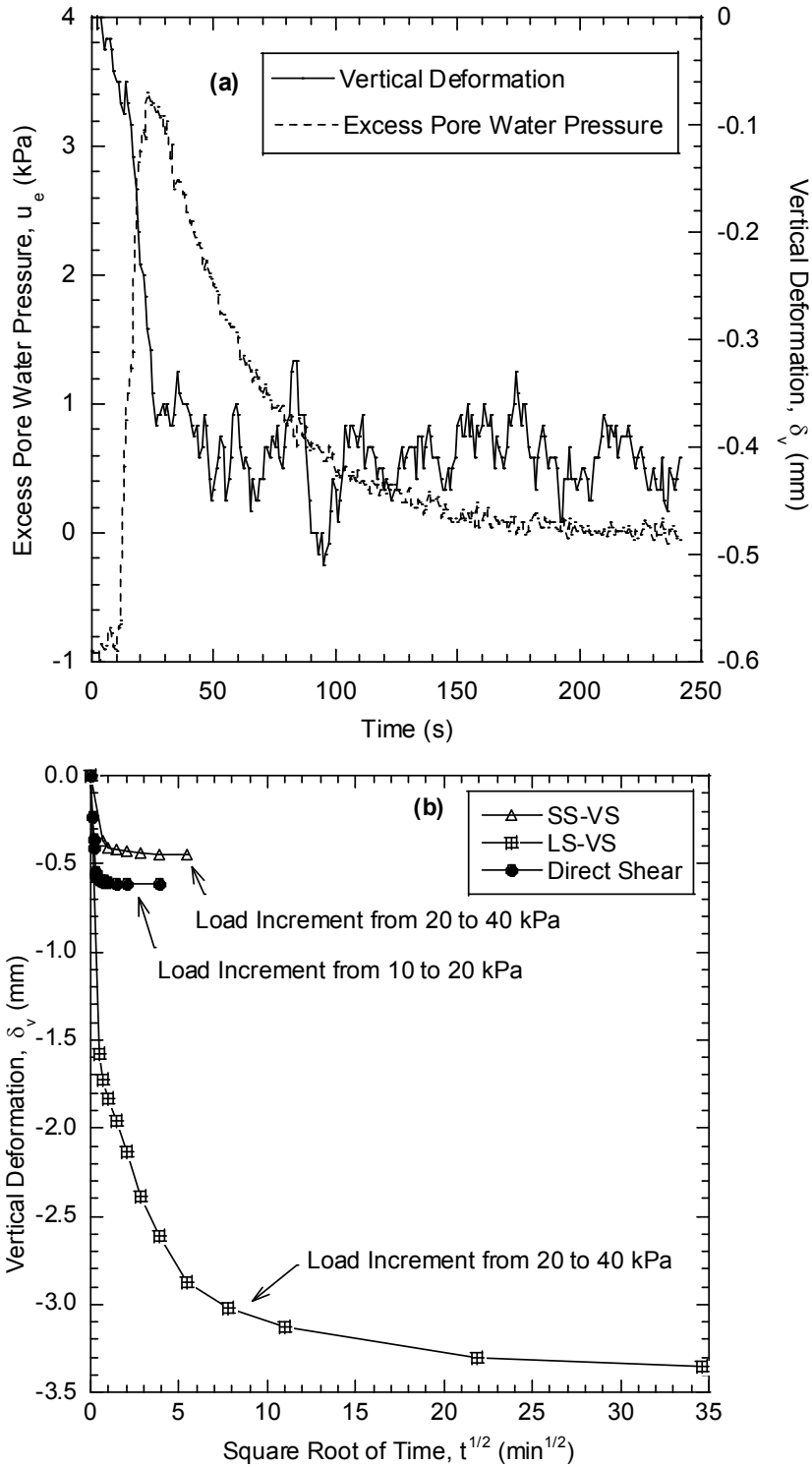
Fig. 4.3. (a) Temporal relationships of excess pore water pressure and vertical deformation the seepage induced consolidation test on SICT_2 based on vertical loading from vertical effective stress (σ_v') = 20 kPa to σ_v' = 40 kPa on CCP. (b) Relationships of vertical deformation versus square root of time for select σ_v' loading increments in small-scale vane shear (SS-VS), large-scale vane shear (LS-VS), and direct shear test on CCP.
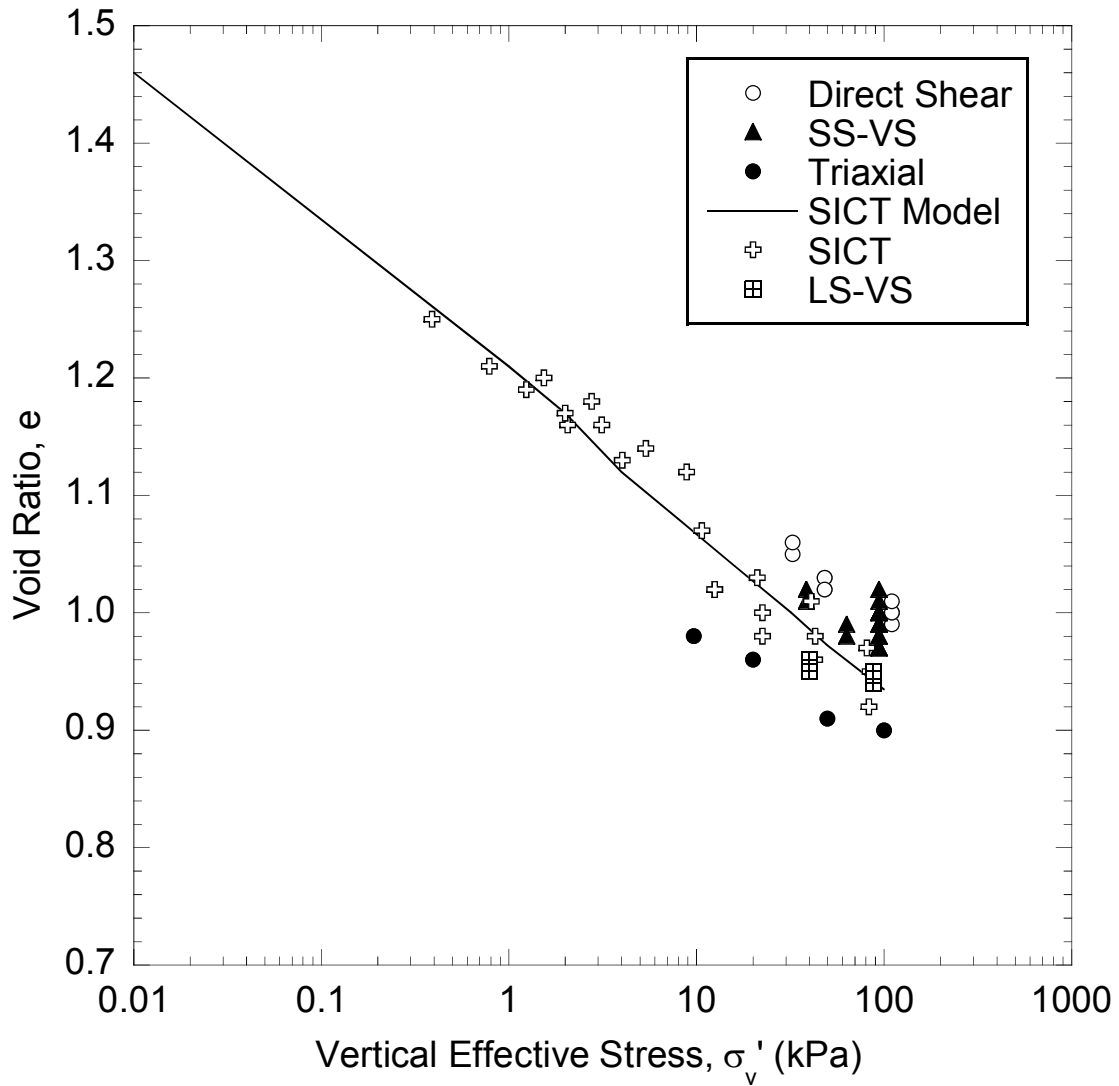
Fig. 4.4. Compilation of void ratio versus vertical effective stress data at the end of consolidation for test specimens prepared in seepage-induced consolidation tests (SICT), direct shear, triaxial, small-scale vane shear (SS-VS), and large-scale vane shear (LS-VS) on CCP.
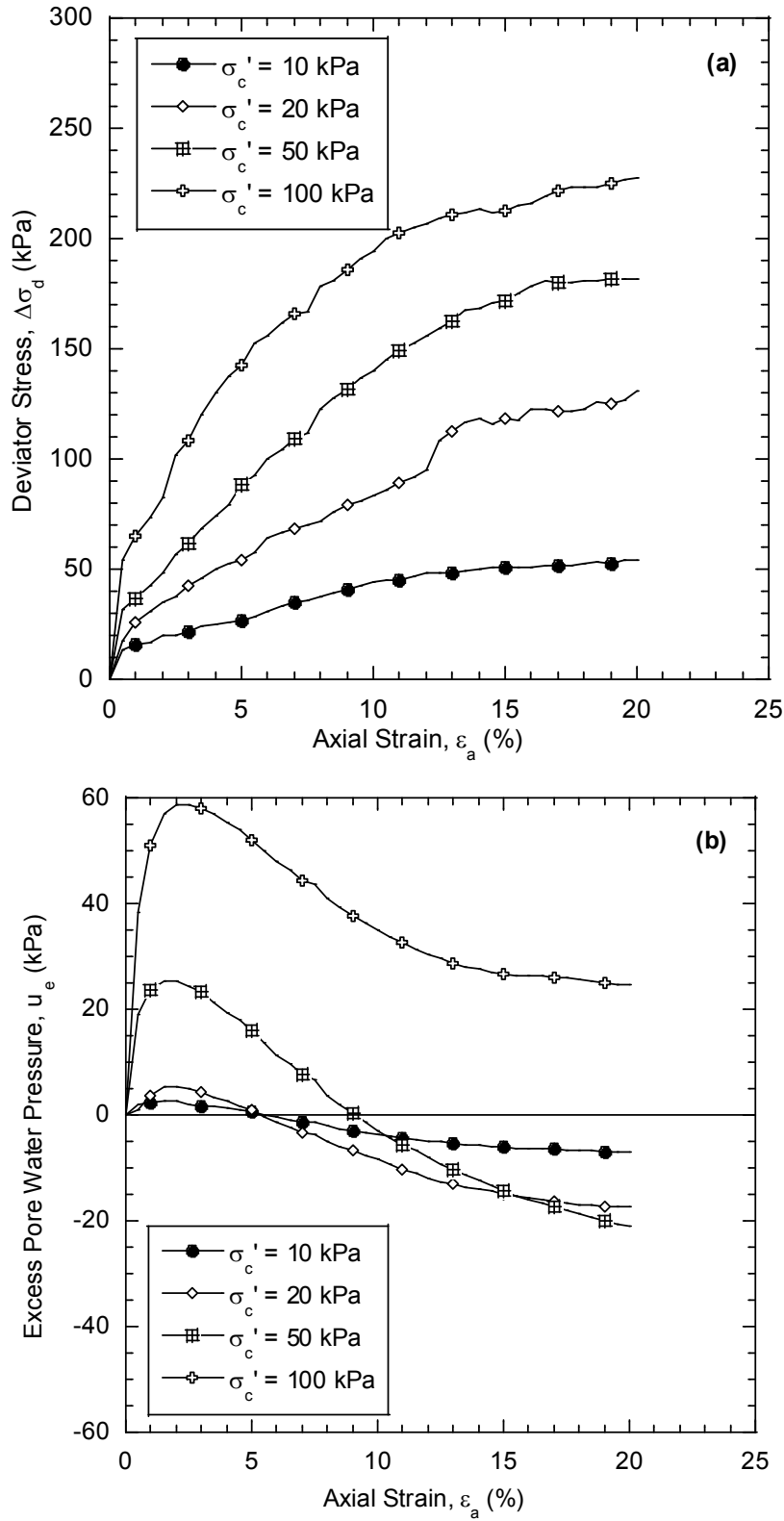
Fig. 4.5. Relationships of (a) deviator stress and (b) excess pore water pressure versus axial strain for consolidated undrained triaxial compression tests on CCP.
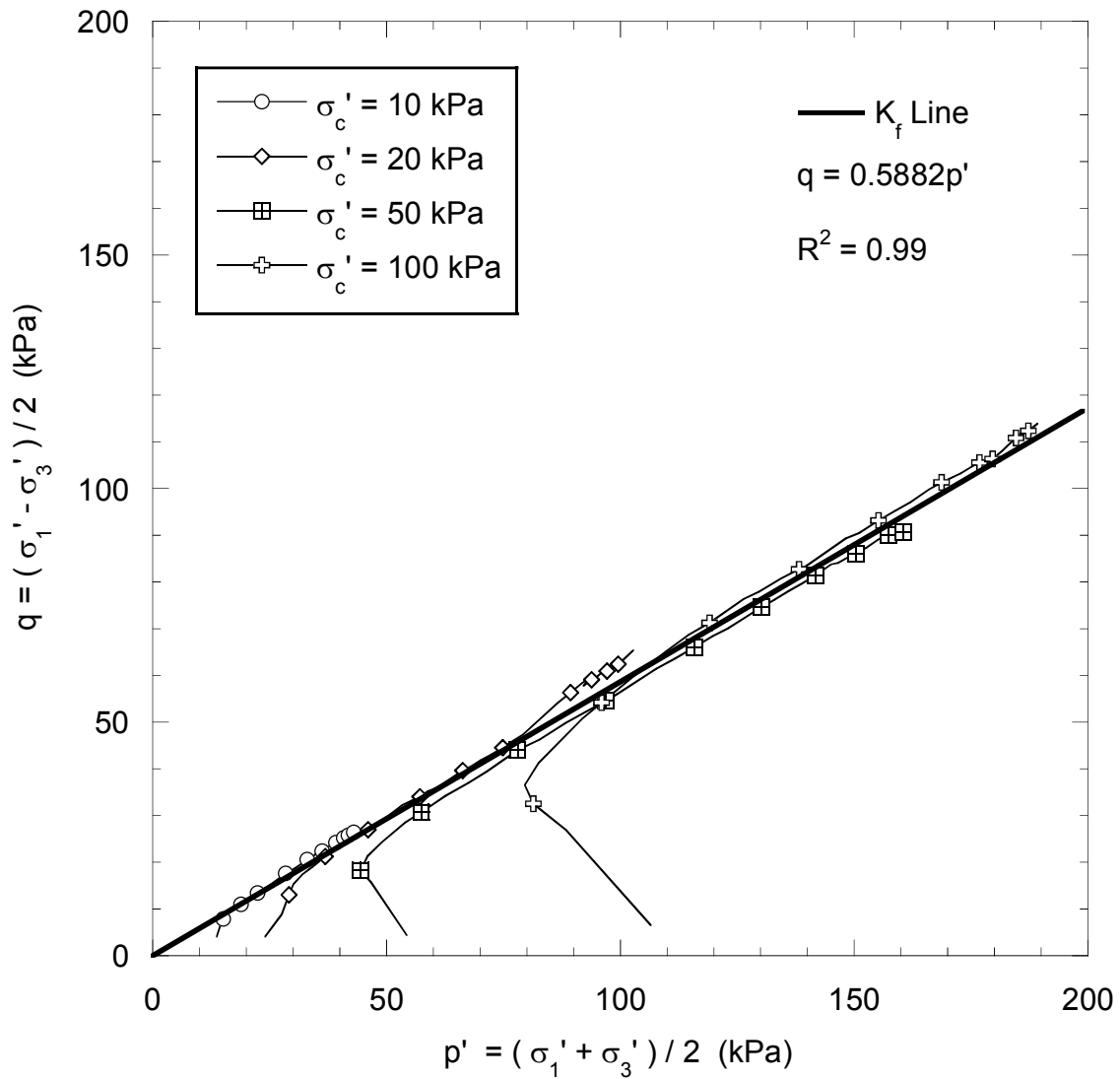
Fig. 4.6. Effective stress paths in *p'-q* space for consolidate undrained triaxial compression tests on CCP. K_f line represents the strength envelope and was based on an analysis conducted using the failure criterion of the effective stress paths reaching K_f line.
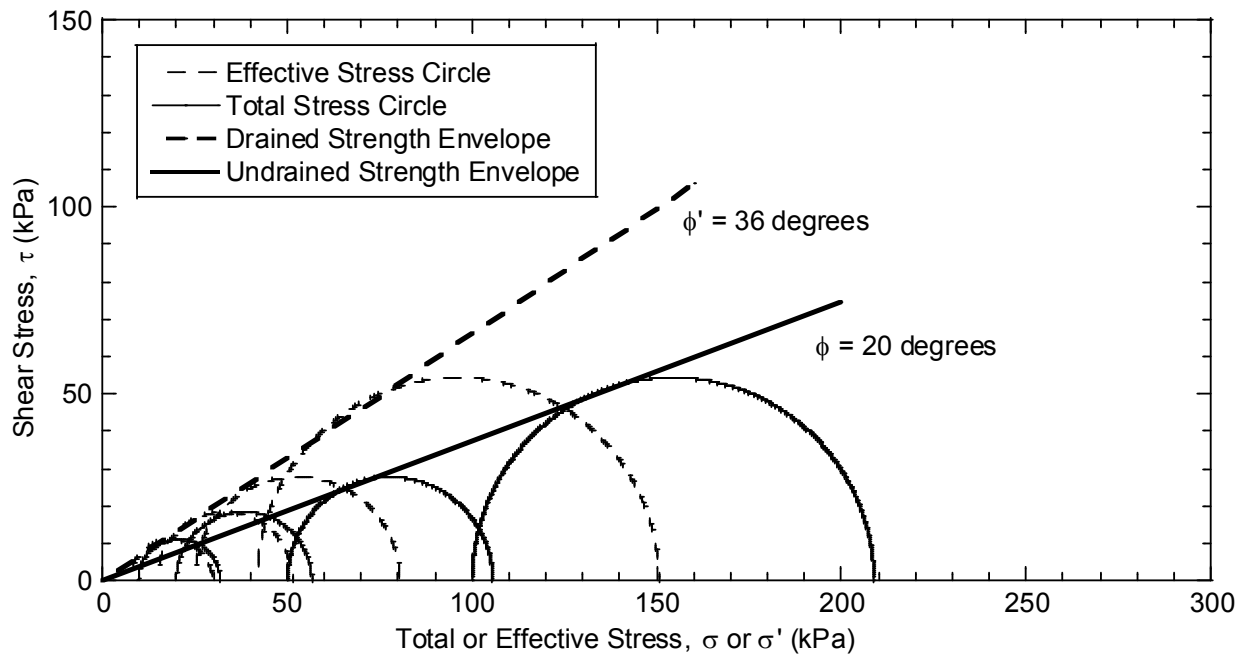
Fig. 4.7. Total and effective stress circles representing failure stress states in the consolidated undrained triaxial compression tests on CCP and best-fit drained and undrained strength envelopes. Failure stress states were based on the effective stress paths reaching the K_f line in *p'-q* space (Fig. 4.6)
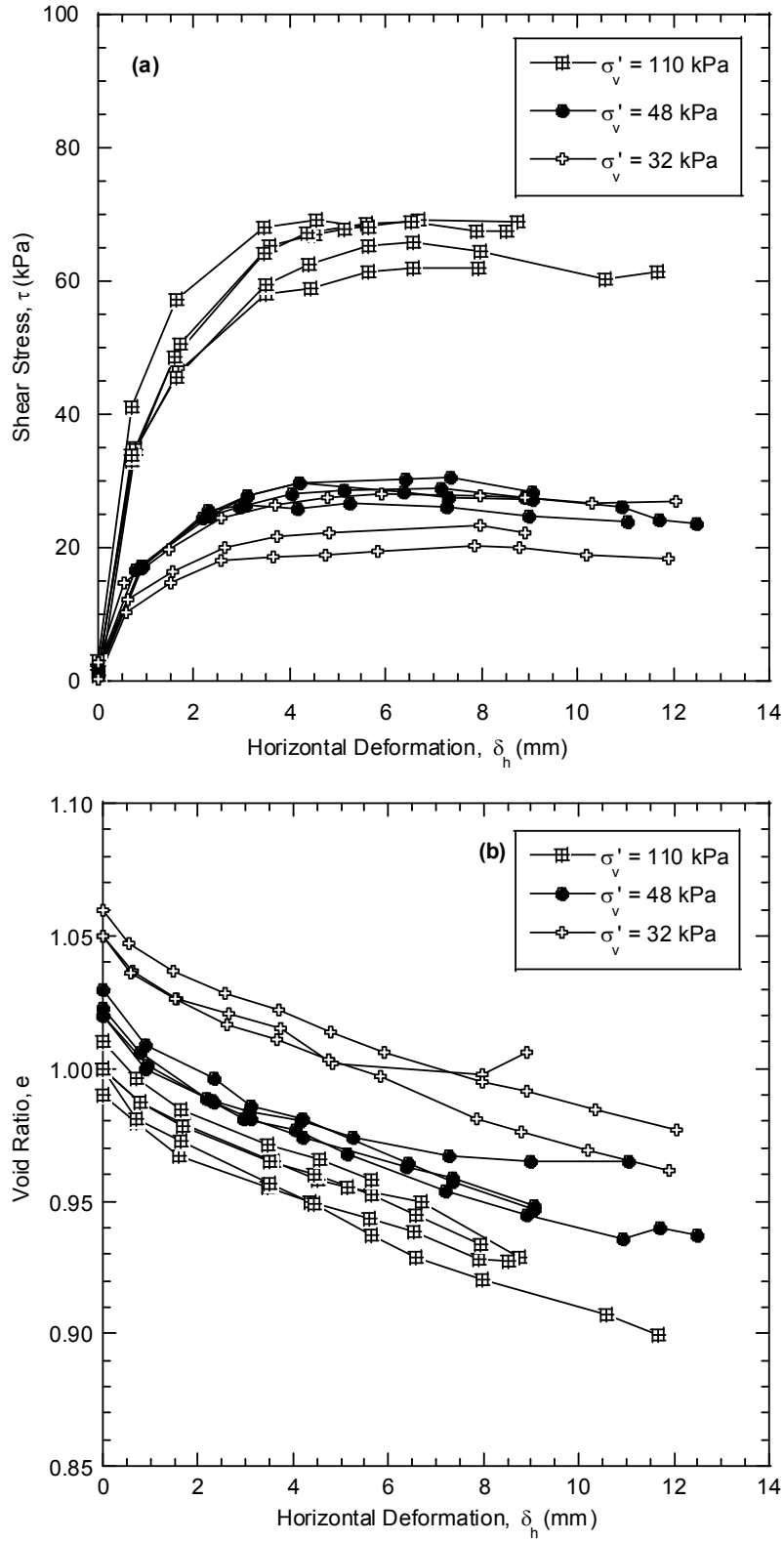
Fig. 4.8. Relationships of (a) shear stress and (b) vertical deformation versus horizontal deformation for consolidated drained direct shear tests on CCP.
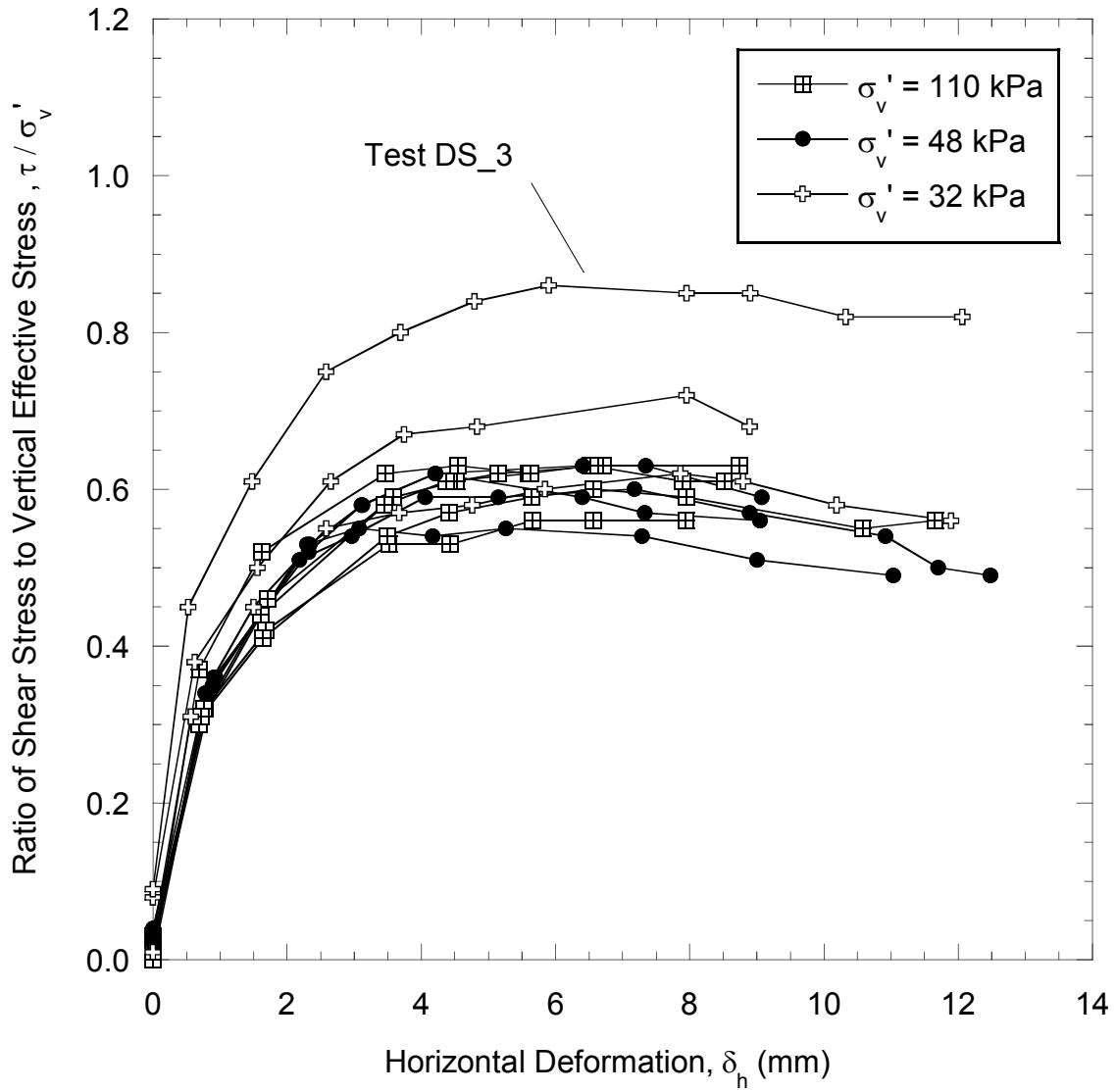
Fig. 4.9. Relationships of the shear stress to vertical effective stress ratio versus horizontal displacement for consolidate drained direct shear tests on CCP.
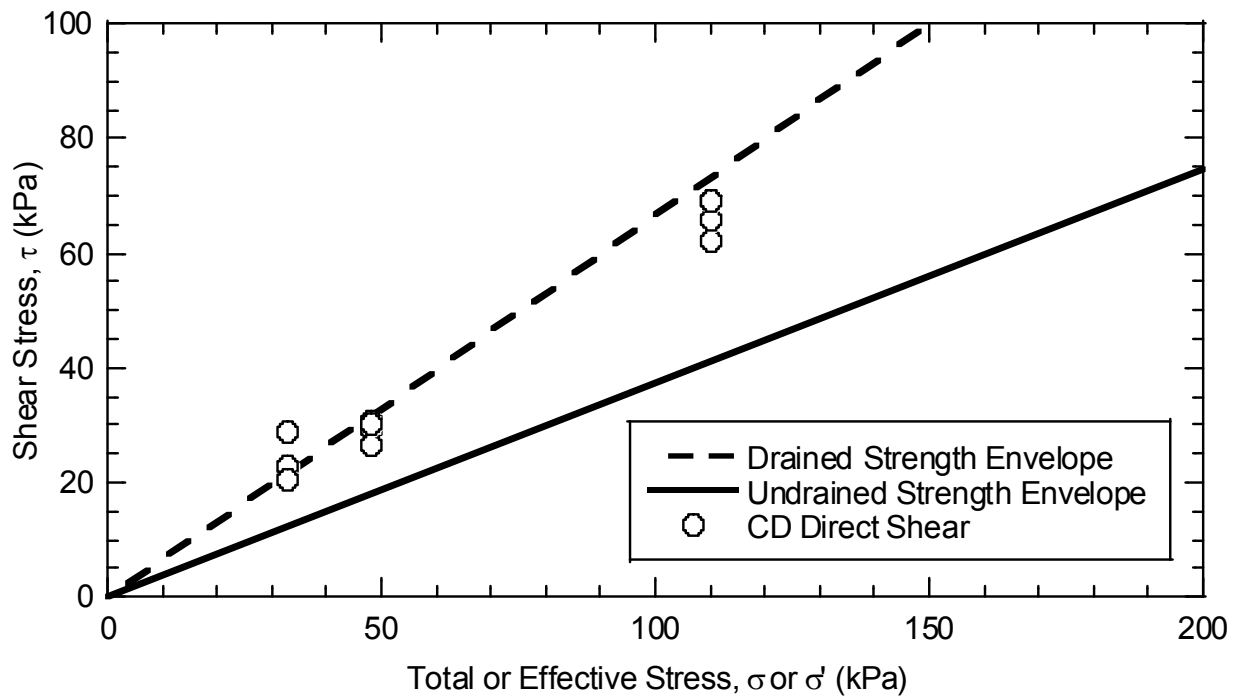
**Fig. 4.10.** Comparison of shear stress and effective vertical stress at failure from direct shear tests on CCP with drained and undrained strength envelopes developed from consolidated undrained triaxial compression tests on CCP.
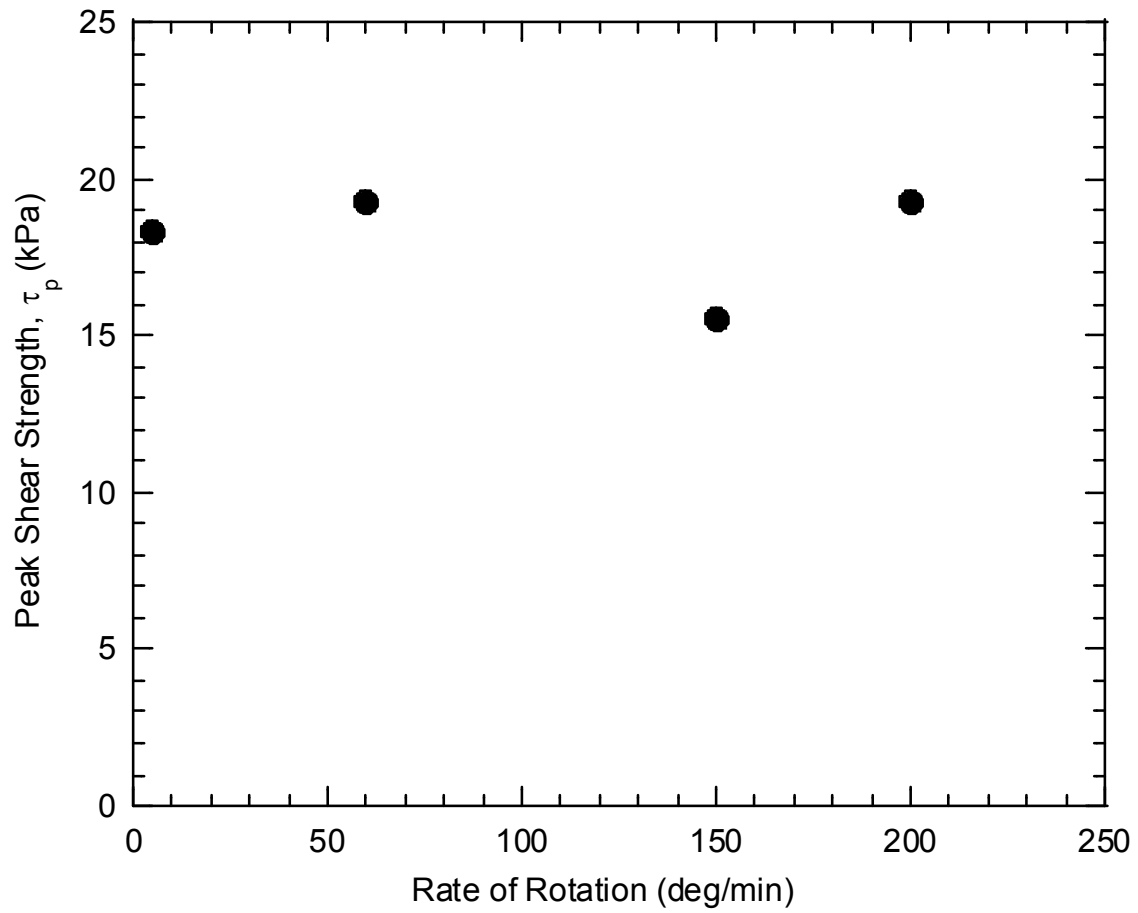
Fig. 4.11. Relationship of peak shear strength versus rate of rotation for small-scale vane shear tests on CCP conducted under a vertical effective stress (σ_v') = 95 kPa.
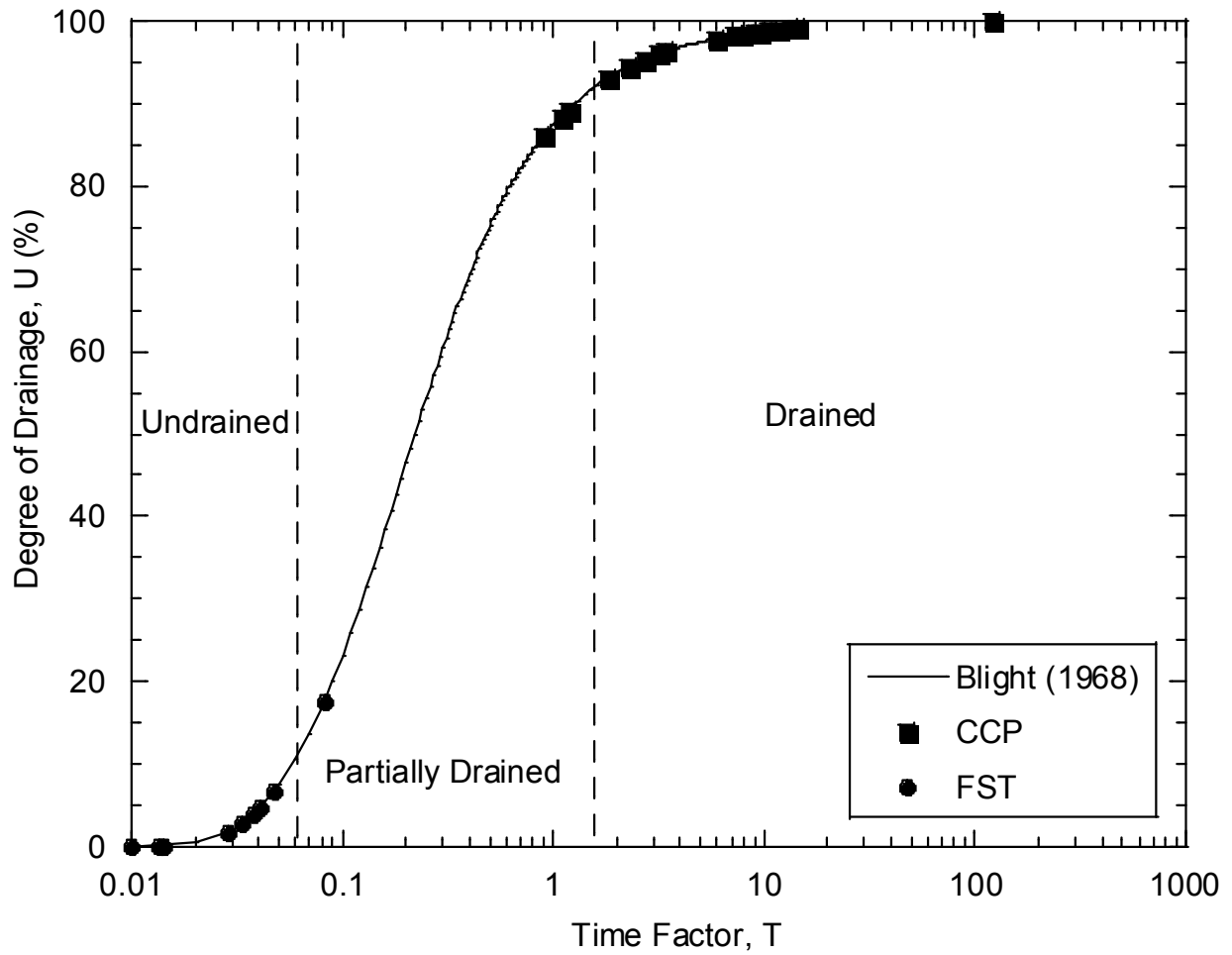
Fig. 4.12. Relationship of degree of drainage versus time factor (Blight, 1968) showing data from SS-VS tests.
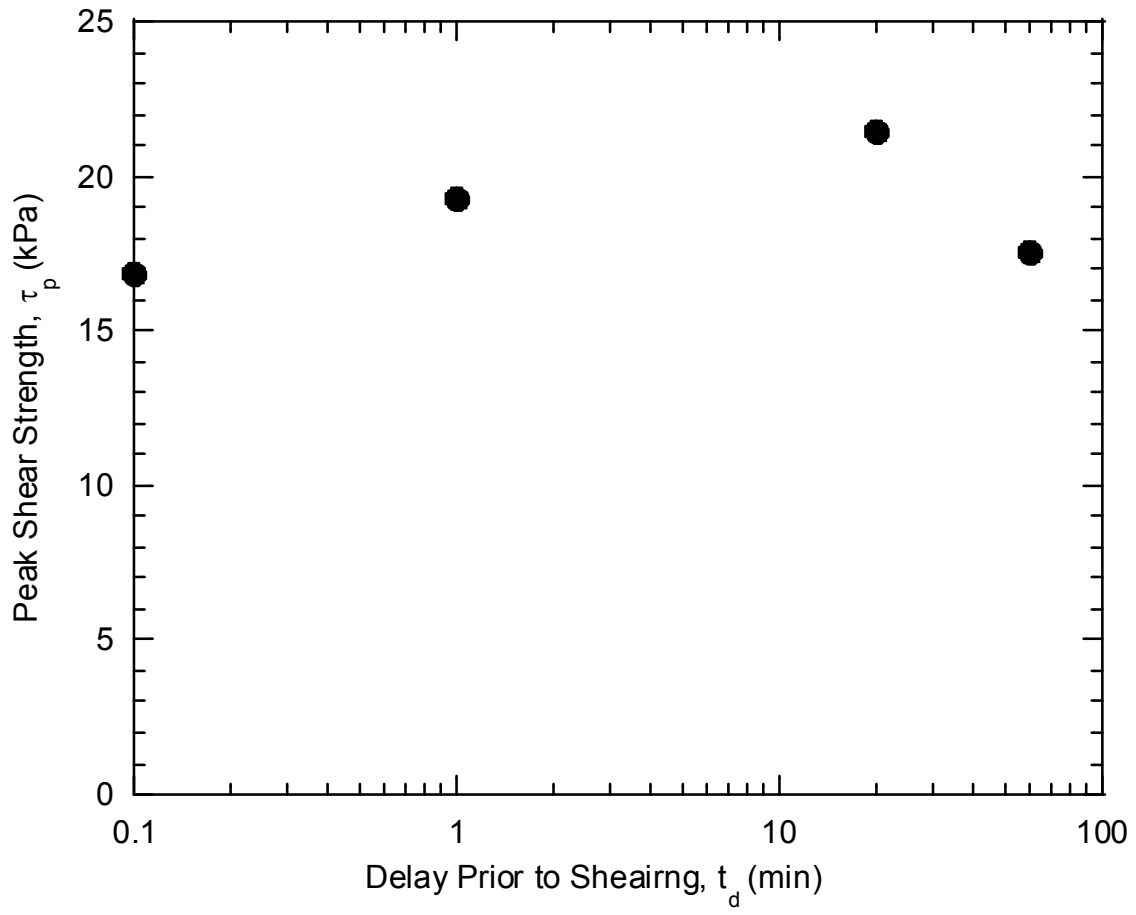
Fig. 4.13. Relationship of peak shear strength versus the time delay prior to shearing for small-scale vane shear tests on CCP conducted under a vertical effective stress (σ_v') = 95 kPa.
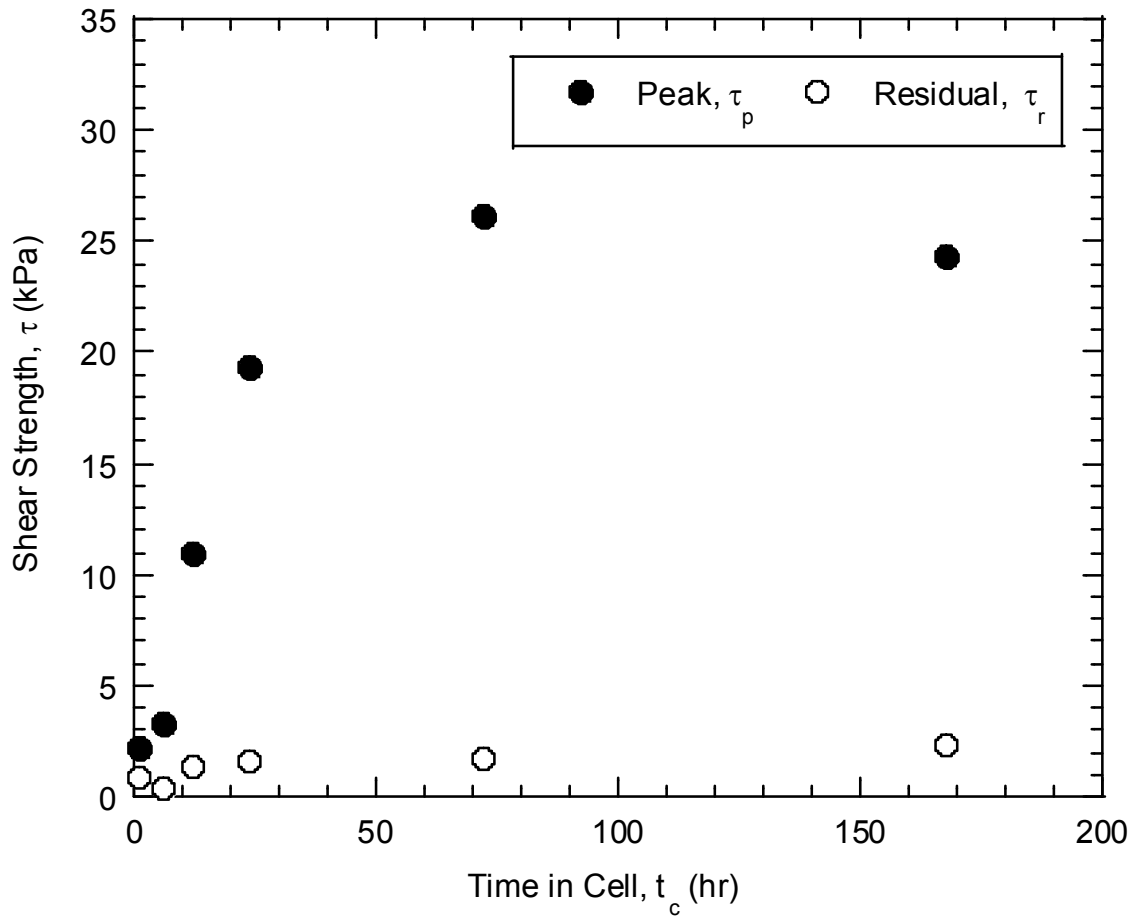
**Fig. 4.14.** Relationship of peak shear strength and residual shear strength versus specimen time in the consolidation cell under a constant vertical effective stress (σ_v') for small-scale vane shear tests on CCP conducted under a σ_v' = 95 kPa.
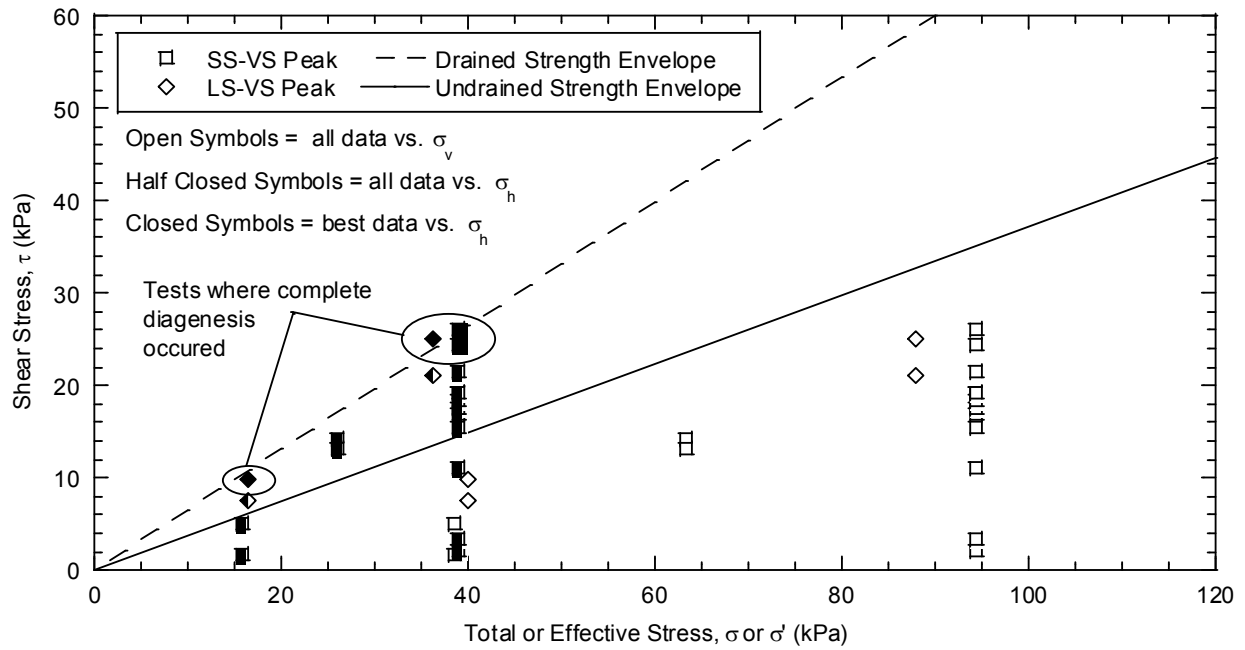
Fig. 4.15. Comparison between shear strength measured with small-scale vane shear (SS-VS), large-scale vane shear (LS-VS), and the drained and undrained strength envelopes developed from consolidated undrained triaxial tests on CCP. Shear strength for SS-VS and LS-VS are plotted relative to the vertical effective stress (σ_v') at the end of consolidation and the lateral effective stress (σ_h') assuming no excess pore pressure development during shear.
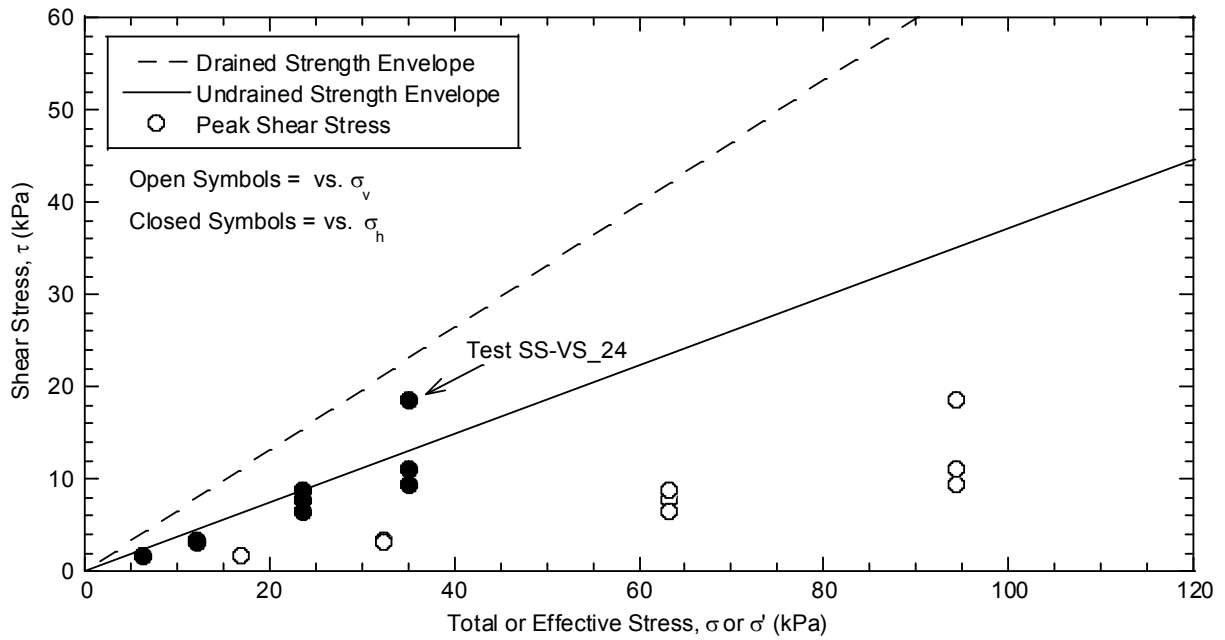
Fig. 4.16. Comparison between shear strength measured with small-scale vane shear (SS-VS) on FST in this study and drained and undrained strength envelopes for FST developed from consolidated undrained triaxial compression tests in Hamade (2017). Shear strength for SS-VS are plotted relative to the vertical effective stress (σ_v') at the end of consolidation and the lateral effective stress (σ_h') computed based on pre-shear conditions.

CHAPTER 5: SUMMARY, CONCLUSIONS AND FUTURE WORK

5.1 Summary and Conclusions

Shear strength of CCP was evaluated with a series of CU triaxial compressions tests, direct shear tests, SS-VS tests, and LS-VS tests. Shear strength measurements from vane shear were compared to drained and undrained strength envelopes developed from CU triaxial compression tests. Effects of the following variables on vane shear strength were evaluated using the SS-VS test: (i) rate of vane rotation, (ii) time delay between vane insertion and beginning rotation (t_d), and (iii) elapsed time under the final σ_v' (t_c). In addition, the shear strength of FST was evaluated using SS-VS tests and compared to drained and undrained strength envelopes previously developed using CU triaxial tests. The following observations and conclusions were drawn from this study.

- CCP had low compressibility and most water was released from the slurry during sedimentation and self-weight consolidation. Hydraulic conductivity ranged between 6 x 10^{-7} m/s and 2 x 10^{-7} m/s, and was relatively insensitive to changes in σ_v'. The c_v for CCP was 1.25 m^2/d, indicating that pore water pressure dissipated rapidly.

- Shear strength of CCP measured in CU triaxial compression and direct shear showed good agreement of drained shear strength. The effective stress friction angle (ϕ') measured in triaxial compression was 36°. Modest differences between failure stress states in direct shear and the drained strength envelope from triaxial compression were attributed to different stress conditions and isotropic consolidation leading to a denser specimen in the triaxial tests.

- Results of SS-VS tests on CCP support that rate of rotation and time delay between vane insertion and beginning rotation had no influence on the measured shear strength. This was attributed to the small vane diameter and high c_v leading to undrained conditions,

even in tests with high rate of rotation (280 °/min) and short time delay prior to beginning rotation (0 min).

- Data from SS-VS tests also illustrated that CCP shear strength increased with time after completion of consolidation. Shear strength increased an order of magnitude from t_c = 1 hr to t_c = 72 hr. This strength increase was attributed to diagenesis, whereby chemical reactions within the CCP increased shear strength of the material.

- The SS-VS and LS-VS tests on CCP showed good agreement when similar experimental conditions existed. In particular, peak shear strength measured in SS-VS and LS-VS compared favorably to the drained strength envelope established in CU triaxial compression when diagenesis was accurately captured in vane shear. The closer agreement with drained strength and overestimation of undrained shear strength in vane shear tests on CCP was attributed to dissipation of excess pore water pressure during testing that led to an increase in measured peak shear strength.

- The SS-VS tests on FST showed good agreement with the undrained strength envelope for FST established via CU triaxial compression tests. This close comparison of peak shear strength measured via vane shear on FST to undrained shear strength demonstrated that by following ASTM standards for vane shear testing, the undrained strength of soft materials with low permeability can be accurately measured.

5.2 Future Work

The present research evaluated the shear behavior of CCP using triaxial, direct shear, and vane shear tests. Further research should consider the effects of drainage conditions during vane shear tests using a larger diameter vane and an electrical torque transducer. The larger vane will provide a longer drainage path, potentially leading to undrained conditions during shear, and the electrical torque transducer will provide data to develop relationships of shear stress

versus deformation. Furthermore, conducting slower SS-VS tests on FST will also be useful to further understand the drainage conditions during vane shear tests. For example, a rate of rotation = 5 º/min would be expected to yield drained or partially drained behavior.

Additional testing should be conducted on CCP to better understand the effect of diagenesis on shear strength. The following tests should be considered: (i) conduct SS-VS tests after longer t_c (e.g., 28 days), and (ii) investigate the effect of wet-dry cycling on diagenesis. Research focusing on the unsaturated shear strength behavior of CCP will also be beneficial. Dewatering of CCP impoundments via pumping is a common method for increasing shear strength to mobilize construction equipment onto ponded CCP. Therefore, understanding how the vane shear test applies to unsaturated CCP will enhance our understanding of the development of shear strength in unsaturated CCP.

REFERENCES

ARTBA, 2015. *Production and Use of Coal Combustion Products in the U.S.,* Washington, D.C.: ARTBA.

Blight, G. E., 1968. A Note on Field Vane Testing of Silty Soils. *Canadian Geotechnical Journal,* 5(3), 142-149.

Brandon, T. L., Rose, A. T. & Duncan, M., 2006. Drained and Undrained Strength Interpretation for Low-Plasticity Silts. *Journal of Geotechnical and Geoenvironmental Engineering,* 132(2), 250-257.

Cadling, L. & Odenstad, S., 1948. The Vane Borer: an Apparatus for Determining the Shear Strength of Clay Soils directly in the Ground. *Royal Swedish Geotechnical Institute Proceedings No. 2.*

Carlson, L., 1948. Determination In Situ of the Shear Strength of Undisturbed Clay by means of a Rotating Auger. *Proceedings of the 2nd International Conference on Soil Mechanics and Foundation Engineering,* Volume 1, 265-270.

Chandler, R. J., 1988. The In-Situ Measurement of the Undrained Shear Strength of Clays Using the Field Vane. In: A. F. Richards, ed. *Vane Shear Strength Testing in Soils: Field and Laboratory Studies, ASTM STP 1014.* Philadelphia: American Society for Testing and Materials, 13-44.

Donald, I. B., Jordan, D. O., Parker, R. J. & Toh, C. T., 1977. The Vane Test - A Critical Appraisal. *Proceedings of the 9th International Conference on Soil Mechanics and Foundation Engineering,* Volume 1, 81-88.

EPA, 2016. *EPA Response to Kingston TVA Coal Ash Spill.* Available at: https://www.epa.gov/tn/epa-response-kingston-tva-coal-ash-spill [Accessed 13 May 2018].

EPA, 2018. *Coal Ash (Coal Combustion Residuals, or CCR).* Available at: https://www.epa.gov/coalash [Accessed 2 April 2018].

EPRI, 2012. *Geotechnical Properties of Fly Ash and Potential for Static Liquefaction: Volume 1 - Summary and Conclusions,* Palo Alto, CA: EPRI.

Evans, D., Whysner, K., Scalia, J. & Bareither, C., 2017. *Work Area Quantification Processes to Guide CCR Construction Programs.* Lexington, KY, World of Coal Ash Conference.

Gang, D., 2014. *Kingston coal ash spill: 5 years, $1 billion in cleanup and no regulations later.* [Online]
Available at: https://www.tennessean.com/story/news/2013/12/20/kingston-coal-ash-spill-5-years-1-billion-in-cleanup-and-no-regulations-later/4153801/
[Accessed 13 May 2018].

Hamade, M., 2017. *Undrained Shear Behavior of Mixed Mine Waste Rock and Tailings,* Master of Science Thesis, Colorado State University, Fort Collins.

Heidrich, C., Feuerborn, H.-J. & Weir, A., 2013. *Coal Combustion Products: a Global Perspective.* Lexington, KY, 2013 World of Coal Ash Conference.

Jehring, M. & Bareither, C. A., 2016. Tailings composition effects on shear strength behavior of co-mixed mine waste rock and tailings. *Acta Geotechnica,* 11(5), 1147-1166.

Kouretzis, G., Pineda, J., Krabbenhoft, K. & Wilson, L., 2017. Interpretations of Vane Shear Tests for Geotechnical Stability Calculations. *Canadian Geotechnical Engineering,* Volume 54, 1775-1780.

Lefebvre, G., Ladd, C. C. & Pare, J. J., 1988. Comparison of Field Vane and Laboratory Undrained Shear Strength in Soft Sensitive Clays. In: A. F. Richards, ed. *Vane Shear Strength Testing in Soils: Field and Laboratory Studies, ASTM STP 1014.* Philadelphia: American Society for Testing and Materials, 233-246.

Liu, J.-C. & Znidarcic, D., 1991. Modeling One-Dimensional Compression Characteristics of Soils. *Journal of Geotechnical Engineering,* 117(1), 162-169.

McCarthy, G., Grier, D., Wisdom, M., Peterson, R., Lerach, S., Jarabek, R., Walsh, J. & Winburn, R., 1999. *Coal Combustion By-Product Diagenesis II.* University of Kentucky, Lexington, KY, International Ash Utilization Symposium.

Menzies, B. K. & Merrifield, C. M., 1980. Measurements of Shear Stress Distribution on the Edges of a Shear Vane Blade. *Geotechnique,* 30(3), 314-318.

Morris, P. H. & Williams, D. J., 2000. A Revision of Blight's Model of Field Vane Testing. *Canadian Geotechnical Journal,* Volume 37, 1089-1098.

Quiros, G. W. & Young, A. G., 1988. Comparison of Field Vane, CPT, and Laboratory Strength Data at Santa Barbara Channel Site. In: A. F. Richards, ed. *Vane Shear Strength Testing in Soils: Field and Laboratory Studies, ASTM STP 1014.* Philadelphia: American Society for Testing and Materials, 306-317.

Reid, D., 2016. Effect of Vane Rotation on Shear Vane Results in a Silty Tailings. *5th International Conference on Geotechnical and Geophysical Site Characterization,* Volume 2, 369-374.

Robertson, P. K., 2009. Interpretation of Cone Penetration Tests - a Unified Approach. *Canadian Geotechnical Journal,* Volume 46, 1337-1355.

Skempton, A. W., 1948. A Study of the Geotechnical Properties of Some Post-Glacial Clays. *Geotechnique,* 1(1), 1-16.

Tian, Z., 2017. *Seepage Induced Consolidation Test on Mine Tailings,* Master of Science Thesis, Colorado State University, Fort Collins.

Wang, S. & Luna, R., 2012. Monotonic Behavior of Mississippi River Valley Silt in Triaxial Compression. *Journal of Geotechnical and Geoenvironmental Engineering,* 138(4), 516-525.